Available online at www.sciencedirect.com
ScienceDirect
Journal of Sound and Vibration 323 (2009) 292–312
JOURNAL OF SOUND AND VIBRATION
www.elsevier.com/locate/jsvi

Symmetry of the Poincaré map and its influence on bifurcations in a vibro-impact system

Y. Yue*, J.H. Xie, H.D. Xu

State Key Laboratory of Traction Power, Southwest Jiaotong University, Chengdu 610031, China

Received 6 February 2007; received in revised form 14 March 2008; accepted 30 November 2008
Handling Editor: L.G. Tham

Abstract

Symmetric period $n-2$ motion of a three-degree-of-freedom (3-dof) vibro-impact system with symmetric rigid constraints is considered. The Poincaré map of the system is established, and the symmetric fixed point of the Poincaré map corresponds to the associated symmetric period $n-2$ motion. It is shown that the Poincaré map exhibits some symmetry property, and can be expressed as the second iteration of another unsymmetric implicit map. The symmetry of the Poincare map influence bifurcation behaviors in vibro-impact system significantly, and suppresses not only period-doubling bifurcation, but also Hopf–flip bifurcation and pitchfork–flip bifurcation. Based on the second iteration of another unsymmetric implicit map, the normal forms in the case of Hopf–Hopf bifurcation and Hopf bifurcation satisfying 1:2 resonant conditions are obtained. By numerical simulation, general Hopf bifurcation, Hopf–Hopf bifurcation and Hopf bifurcation satisfying 1:2 resonant conditions of the symmetric period $n-2$ motion are represented. However, period-doubling bifurcation, Hopf–flip and pitchfork–flip bifurcation have not been obtained, which reflects upon the effect of the symmetry property on possible bifurcations. It is interesting that the system can exhibit both the characteristic of 1:2 resonance and that of torus $\mathbf{T}^2$ under some parameter combination, and $2 \times \mathbf{T}^1$ torus is also obtained.

1. Introduction

Because of the existence of impacts, the vibro-impact system is discontinuous and strongly nonlinear, such as hammer-like devices, rotor-casing dynamical systems, heat exchangers, fuel elements of nuclear reactor, gears, piping systems, wheel–rail interaction of high speed railway coaches. Researches into the dynamic behavior of vibro-impact systems have important significance in optimization design of machinery and noise suppression. Hence, the complication of the dynamics of vibro-impact system has received great attention. Early studies on vibro-impact system mainly focused on single-degree-of-freedom system, see Refs. [1–10]. Budd and Dux [8] proved that the periodic motion of the single-degree-of-freedom vibro-impact system cannot have Hopf bifurcation. In recent years, many researchers investigated some two- and three-degree of

*Corresponding author. Fax: +86 28 87634460.
E-mail addresses: peak8668@yahoo.com.cn (Y. Yue), jhxie2000@126.com (J.H. Xie).

0022-460X/$ - see front matter
doi:10.1016/j.jsv.2008.11.047

freedom (3-dof) of vibro-impact systems, and found that these vibro-impact systems can exhibit rich dynamic behavior, and have various bifurcations, such as period-doubling bifurcation [11,12], Hopf bifurcation [13,14]. Besides, there are some studies on calculation of Lyapunov exponents [15,16], controlling chaos [17,18] and rising phenomena and the multi-sliding bifurcation [19] in systems with impacts. Dynamics of vibro-impact system in two cases of resonance (1:3 and 1:4 resonance) was also studied by Ding and Xie [20]. Luo and Chen [21] presented an idealized, piecewise linear system to model the vibration of gear transmission systems, and developed the analytical predictions of periodic motion based on the mapping structures. It should be mentioned that codimension between two bifurcation of multi-degree-of-freedom vibro-impact systems has attracted more and more attention, see Refs. [22–27]. Xie and Ding [25] considered Hopf–Hopf bifurcation of a 3-dof vibro-impact system. When two pairs of complex conjugate eigenvalues of the Jacobian matrix of the map at fixed point cross the unit circle simultaneously, the six-dimensional Poincaré map was reduced to its four-dimensional normal form by the center manifold and the normal form methods. It was shown that there are torus $\mathbf{T}^1$ and $\mathbf{T}^2$ bifurcation under some parameter combinations. In Ref. [27], an inertial shaker as a vibratory system with impact was considered. Dynamics of the system was studied with special attention to interaction of Hopf and period doubling bifurcations. The four-dimensional map was reduced to a three-dimensional normal form by the center manifold theorem and the theory of normal forms. It was shown that there exist curve doubling bifurcation, Hopf bifurcation of 2–2 fixed points as well as period doubling bifurcation and Hopf bifurcation of 1–1 fixed points near the critical point.

A great deal of issues on vibro-impact dynamics interest many researchers greatly, but little attention has been paid to the symmetry characteristic of the Poincaré map and its influence on possible bifurcations in vibro-impact systems. In Ref. [28], we considered a two-degree-of-freedom (2-dof) vibro-impact system with symmetric rigid constraints, and described the symmetry of Poincaré map. It was shown that if the Jacobian matrix of the Poincaré map at the fixed point has a real eigenvalue crossing the unit circle at $+1$, the symmetric fixed point will bifurcate into two antisymmetric fixed points which have the same stability via pitchfork bifurcation. While the control parameter changes continuously, the two antisymmetric fixed points will give birth to two synchronous bifurcation sequences.

In this paper, we expand the symmetry of Poincaré map of the 2-dof vibro-impact system discussed in Ref. [28] to a 3-dof vibro-impact system with symmetric rigid constraints, and pay more attention to the effect of the symmetry of Poincaré map on possible bifurcations. Based on the second iteration of another unsymmetric map, we obtain the normal forms of Hopf–Hopf bifurcation and Hopf bifurcation satisfying 1:2 resonance conditions. It is interesting that the system can exhibit both the characteristic of 1:2 resonance and that of torus $\mathbf{T}^2$ under some parameter combination.

2. Mechanical model

A 3-dof system with symmetric rigid constraints is shown in Fig. 1. The system has three masses M_1, M_2 and M_3. M_2 and M_3 are connected to rigid planes via two linear springs K_2 and K_3, and two linear viscous dashpots

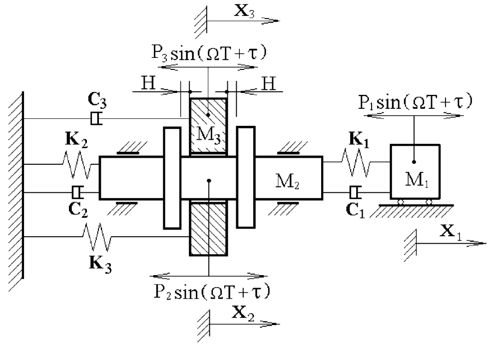

Fig. 1. A three-degree-of-freedom vibro-impact system with symmetric rigid constraints.

C_2 and C_3, respectively. M_1 is connected to M_2 via linear spring K_1 and linear viscous dashpot C_1. The excitations on three masses are harmonic with amplitudes P_1, P_2 and P_3. For small forcing amplitudes the system undergoes simple oscillations and behaves as a linear system. However, as the amplitudes increased, M_3 begins to collide with two stops of M_2, and the system becomes discontinuous and strongly nonlinear. The impact is described by a coefficient of restitution R. It is assumed that the duration of impact is negligible compared to the period of the force, and the friction between M_3 and M_2 is negligible, too. C_1 and C_2 are assumed as proportional damping.

Between any two consecutive impacts, the non-dimensional differential equations of motion are given by

$$\left.\begin{aligned} &u_{m1}\ddot{x}_1 + 2u_{c1}\zeta(\dot{x}_1 - \dot{x}_2) + u_{k1}(x_1 - x_2) = u_{f1}f\sin(\omega t + \tau), \\ &u_{m2}\ddot{x}_2 + 2(u_{c1} + u_{c2})\zeta\dot{x}_2 - 2u_{c1}\zeta\dot{x}_1 + (u_{k1} + u_{k2})x_2 - u_{k1}x_1 = u_{f2}f\sin(\omega t + \tau), \\ &u_{m3}\ddot{x}_3 + 2u_{c3}\zeta\dot{x}_3 + u_{k3}x_3 = u_{f3}f\sin(\omega t + \tau), \end{aligned}\right\} \tag{1}$$

where the non-dimensional variables and parameters are $t = T\sqrt{K_3/M_3}$, $\zeta = C_3/2\sqrt{K_3M_3}$, $\omega = \Omega\sqrt{M_3/K_3}$, $f = P_3/P_0$, $u_{mi} = M_i/M_3$, $u_{ki} = K_i/K_3, u_{ci} = C_i/C_3, u_{fi} = P_i/P_3$, $x_i = X_iK_3/P_0$, $i = 1,2,3$, and $P_0 = |P_1| + |P_2| + |P_3|$. The phase angle τ is used only to make a suitable choice for the origin of time in the calculation.

When M_3 impacts the left and the right stops of M_2, the non-dimensional displacements of two masses satisfy $|x_2 - x_3| = h$, where $h = K_3H/P_0$. After each impact, the velocities of M_2 and M_3 change according to the impact law:

$$\dot{x}_{2+} = m_1\dot{x}_{2-} + n_1\dot{x}_{3-}, \quad \dot{x}_{3+} = m_2\dot{x}_{2-} + n_2\dot{x}_{3-}, \tag{2}$$

where $m_1 = (u_{m2} - R)/(1 + u_{m2})$, $n_1 = (1 + R)/(1 + u_{m2})$, $m_2 = (u_{m2}(1 + R))/(1 + u_{m2})$, $n_2 = (1 - u_{m2}R)/(1 + u_{m2})$.

In Eqs. (1) and (2), a dot $(\cdot)$ denotes differentiation with respect to the non-dimensional time t. $\dot{x}_{i-}$ and $\dot{x}_{i+}$ represent the non-dimensional velocities of M_i before and after impacting, respectively.

The first and the second differential equations of Eq. (1) are coupling, and the eigenfrequencies can be solved as ω_1 and ω_2. Taking $\boldsymbol{\psi}$ as the canonical model matrix, and making the change of variables $[x_1, x_2]^{\mathrm{T}} = \boldsymbol{\psi}\xi$, the first and the second equations of Eq. (1) become

$$\mathbf{I}\ddot{\xi} + \mathbf{C}\dot{\xi} + \boldsymbol{\Lambda}\xi = \overline{\mathbf{F}}\sin(\omega t + \tau) \tag{3}$$

where $\mathbf{C} = 2\zeta_p\boldsymbol{\Lambda} = \mathrm{diag}[2\zeta_p\omega_1^2, 2\zeta_p\omega_2^2]$, $\overline{\mathbf{F}} = [\overline{f}_1, \overline{f}_2]^{\mathrm{T}} = \boldsymbol{\psi}^{\mathrm{T}}P_k$, $P_k = [u_{f1}f, u_{f2}f]^{\mathrm{T}}$.

Let ϕ_{kj} denotes the element of $\boldsymbol{\psi}$, the general solution of Eq. (1) is given by

$$\left.\begin{aligned} &x_1(t) = \sum_{j=1}^{2}\phi_{1j}(\mathrm{e}^{-\eta_j t}(a_j\cos(\omega_{dj}t) + b_j\sin(\omega_{dj}t)) + A_j\sin(\omega t + \tau) + B_j\cos(\omega t + \tau)), \\ &x_2(t) = \sum_{j=1}^{2}\phi_{2j}(\mathrm{e}^{-\eta_j t}(a_j\cos(\omega_{dj}t) + b_j\sin(\omega_{dj}t)) + A_j\sin(\omega t + \tau) + B_j\cos(\omega t + \tau)), \\ &x_3(t) = e^{-\eta_3 t}(a_3\cos(\omega_{d3}t) + b_3\sin(\omega_{d3}t)) + A_3\sin(\omega t + \tau) + B_3\cos(\omega t + \tau), \end{aligned}\right\} \tag{4}$$

where $\eta_j = \zeta_p\omega_j^2$, $\omega_{dj} = \sqrt{\omega_j^2 - \eta_j^2}$, $j = (1,2)$, $\eta_3 = \zeta$, $\omega_{d3} = \sqrt{1 - \eta_3^2}$, and a_i and b_i are integration constants, A_i and B_i are amplitude constants.

3. Symmetric period *n*–2 motion

Firstly, we give the definition of symmetric period $n-2$ motion, according to which the symmetric period $n-2$ motion can be obtained analytically.

Definition 1. (Symmetric period $n-2$ motion). Let the origin of the time coordinate is displaced to the moment that M_3 impacts the right stop of M_2 ($t = t_0 = 0$). Subsequently, at the moment $t = t_1 = n\pi/\omega$ (n is an odd number), M_3 impacts the left stop. At the moment $t = t_2 = 2n\pi/\omega$, M_3 impacts the right stop once again.

The periodic motion will be called symmetric period n–2 motion if the following relationships are satisfied:

$$x_i(t_1) = -x_i(t_0), \quad \dot{x}_{i+}(t_1) = -\dot{x}_{i+}(t_0), \tag{5.1}$$

$$x_i(t_2) = x_i(t_0), \quad \dot{x}_{i+}(t_2) = \dot{x}_{i+}(t_0), \tag{5.2}$$

where $i = 1,2,3$, and $x_i(t_j)$ and $\dot{x}_{i+}(t_j)$ represent the non-dimensional displacements and velocities of M_i after impacting at the moment t_j ($j = 0,1,2$), respectively.

In other words, after M_3 impacts the right and the left stops, the associated state coordinates are equal in absolute value and opposite in direction. According to the definition, we can easily obtain the following proposition on the existence condition of symmetric period n–2 motion.

Proposition 2. (*Existence of the symmetric period n*–2 *motion*). *If there are initial conditions* $\tau = \tau_0$, $x_i(0) = x_{i0}$, $\dot{x}_{i+}(0) = y_{i0}$, *which result in*

$$\left.\begin{aligned} &x_i(0) = -x_i(t_1),\\ &\dot{x}_{i+}(0) = -\dot{x}_{i+}(t_1),\\ &x_2(0) - x_3(0) = -h,\\ &x_2(t_1) - x_3(t_1) = +h, \end{aligned}\right\} \tag{6}$$

then the symmetric period n–2 *motion of the system exists, and can be expressed by*

$$x_i(t) = \begin{cases} x_i(t), t \in [0, t_1] \\ -x_i(t - t_1), t \in [t_1, t_2] \end{cases}, \quad i = 1, 2, 3. \tag{7}$$

Inserting the general solutions (4) into the boundary conditions (6), after simplification, we obtain

$$\left.\begin{aligned} &m_a a_1 + m_c \cos \tau_0 + m_s \sin \tau_0 + m_h = 0,\\ &n_a a_1 + n_c \cos \tau_0 + n_s \sin \tau_0 + n_h = 0. \end{aligned}\right\} \tag{8}$$

Thus, the phase angle τ_0 and the integration constants can be solved (see Appendix A). Substituting them into the general solution (4), and considering that impacts change the integration constants, we obtain the symmetric period n–2 solution:

$$x_i(t) = \begin{cases} \sum_{j=1}^{2} \phi_{ij}[\mathrm{e}^{-\eta_j t}(a_{ji} \cos(\omega_{dj} t) + b_{ji} \sin(\omega_{dj} t)) + A_j \sin(\omega t + \tau_0) \\ \quad + B_j \cos(\omega t + \tau_0)], \quad t \in [0, t_1]; \\ \sum_{j=1}^{2} \phi_{ij}[\mathrm{e}^{-\eta_j (t-t_1)}(a_{ji} \cos(\omega_{dj}(t - t_1)) + b_{ji} \sin(\omega_{dj}(t - t_1))) + A_j \sin(\omega t + \tau_0) \\ \quad + B_j \cos(\omega t + \tau_0)], \quad t \in [t_1, t_2], \end{cases} \quad i = 1, 2, \tag{9.1}$$

$$x_3(t) = \begin{cases} \mathrm{e}^{-\eta_3 t}[a_{31} \cos(\omega_{d3} t) + b_{31} \sin(\omega_{d3} t)] + A_3 \sin(\omega t + \tau_0) + B_3 \cos(\omega t + \tau_0), \quad t \in [0, t_1]; \\ \mathrm{e}^{-\eta_3 (t-t_1)}[a_{32} \cos(\omega_{d3}(t - t_1)) + b_{32} \sin(\omega_{d3}(t - t_1))] + A_3 \sin(\omega t + \tau_0) + B_3 \cos(\omega t + \tau_0), \quad t \in [t_1, t_2]; \end{cases} \tag{9.2}$$

where a_{jk} ($j = 1,2,3$; $k = 1,2$) are the integration constants determined by the initial conditions after impacting (see Appendix B).

4. Poincaré map and its symmetry

Let $y_i = \dot{x}_i$ denotes the velocity of M_i, Eq. (1) can be rewritten as

$$\left.\begin{aligned}
&\dot{x}_1 = y_1,\\
&\dot{y}_1 = \frac{1}{u_{m1}}[-u_{k1}x_1 + u_{k1}x_2 - 2u_{c1}\zeta y_1 + 2u_{c1}\zeta y_2 + u_{f1}f\ \sin(\omega t + \tau)],\\
&\dot{x}_2 = y_2,\\
&\dot{y}_2 = \frac{1}{u_{m2}}[u_{k1}x_1 - (u_{k1} + u_{k2})x_2 + 2u_{c1}\zeta y_1 - 2(u_{c1} + u_{c2})\zeta y_2 + u_{f2}f\ \sin(\omega t + \tau)],\\
&\dot{x}_3 = y_3,\\
&\dot{y}_3 = \frac{1}{u_{m3}}[-u_{k3}x_3 - 2u_{c3}\zeta y_3 + u_{f3}f\ \sin(\omega t + \tau)].
\end{aligned}\right\} \tag{10}$$

Equivalently:

$$\dot{\mathbf{X}} = \mathbf{F}(\mathbf{X}, t), \tag{11}$$

where $\mathbf{X} = (x_1, y_1, x_2, y_2, x_3, y_3)^{\mathrm{T}}$, and we have

$$\mathbf{F}\left(\mathbf{X}, t + \frac{2\pi}{\omega}\right) = \mathbf{F}(\mathbf{X}, t) \tag{12}$$

and

$$\mathbf{F}\left(-\mathbf{X}, t + \frac{\pi}{\omega}\right) = -\mathbf{F}(\mathbf{X}, t). \tag{13}$$

The phase space of the vibro-impact system is

$$\mathbf{R}^6 \times \mathbf{S}^1 = \{(x_1, y_1, x_2, y_2, x_3, y_3, t) | (x_1, y_1, x_2, y_2, x_3, y_3) \in \mathbf{R}^6, t \in \mathbf{S}^1\}, \tag{14}$$

where $\mathbf{S}^1$ is the $2\pi/\omega$-circle. And the Poincaré section is chosen as

$$\mathbf{\Pi}_0 = \{(x_1, y_1, x_2, y_2, x_3, y_3, t) \in \mathbf{R}^6 \times \mathbf{S}^1 | x_2 - x_3 = -h\}. \tag{15}$$

Subsequently, we define a transformation

$$\mathbf{R} : (x_1, y_1, x_2, y_2, x_3, y_3, t) \mapsto \left(-x_1, -y_1, -x_2, -y_2, -x_3, -y_3, t + \frac{n\pi}{\omega}\right) \tag{16}$$

and a section:

$$\mathbf{\Pi}_1 = \{(x_1, y_1, x_2, y_2, x_3, y_3, t) \in \mathbf{R}^6 \times \mathbf{S}^1 | x_2 - x_3 = +h\}. \tag{17}$$

Now it should be noted that $\mathbf{\Pi}_0$ and $\mathbf{\Pi}_1$ are chosen at the moment after impacting at the right and the left stops, respectively. Hence, in section $\mathbf{\Pi}_0$ and $\mathbf{\Pi}_1$, we have $\dot{y}_i = \dot{y}_{i+}$.

Due to $t \in \mathbf{S}^1$, we have

$$\mathbf{R}^2 = \mathbf{I} \tag{18}$$

where $\mathbf{I}$ is the identity transformation. Let $(x_{1i}, y_{1i}, x_{2i}, y_{2i}, x_{3i}, y_{3i}, t_i)^{\mathrm{T}}$ denote the coordinates vector of point $\mathbf{X}_i$ (i = 1,2). According to Eqs. (13) and (16), we obtain

$$\mathbf{RF}(\mathbf{X}) = \mathbf{F}(\mathbf{RX}). \tag{19}$$

Lemma 3. (*Yue and Xie* [28]). *Let* $\mathbf{X}(\mathbf{X}_0, t)(t = t_0 + \Delta t)$ *be the solution of Eq.* (10) *which starts at the point* $\mathbf{X}_0 \in \mathbf{\Pi}_0$ *between two consecutive impacts* ($\Delta t \in [0, n\pi/\omega)$, *and* $\mathbf{X}(\mathbf{X}_1, t + n\pi/\omega)$ *be the solution of Eq.* (10) *which*

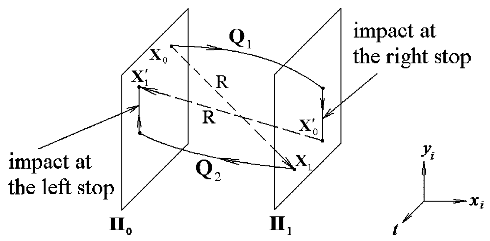

Fig. 2. Schematic diagram of $\mathbf{Q}_1$ and $\mathbf{Q}_2$.

starts at the point $\mathbf{X}_1 = \mathbf{RX}_0 \in \mathbf{\Pi}_1$, *we have*

$$\mathbf{RX}(\mathbf{X}_0, t_0 + \Delta t) = \mathbf{X}(\mathbf{X}_1, t_1 + \Delta t) \tag{20}$$

Supposing that it takes Δt_1 time for the solution which starts at $\mathbf{X}_0 \in \mathbf{\Pi}_0$ to reach the section $\mathbf{\Pi}_1$, and it takes Δt_2 time for the solution which starts at $\mathbf{X}_1 \in \mathbf{\Pi}_1$ to reach the section $\mathbf{\Pi}_0$, we can obtain $\Delta t_1 = \Delta t_2$ [28].

Due to $|x_2 - x_3| = h$ when M_3 impacts the left and the right stops of M_2, we choose $(x_1, y_1, x_2, y_2, y_3, t)$ as the coordinates of $\mathbf{\Pi}_0$ and $\mathbf{\Pi}_1$, and delete the coordinates x_3. As shown in Fig. 2, defining $\mathbf{Q}_1 : \mathbf{\Pi}_0 \to \mathbf{\Pi}_1$ (including an impact) and $\mathbf{Q}_1(\mathbf{X}_0) = \mathbf{X}_0'$, where

$$\left.\begin{aligned} \mathbf{X}_0 &= (x_{10}, y_{10}, x_{20}, y_{20}, y_{30}, t_0) \in \mathbf{\Pi}_0, \\ \mathbf{X}_0' &= (x_{10}', y_{10}', x_{20}', y_{20}', y_{30}', t_0') \in \mathbf{\Pi}_1, \end{aligned}\right\} \tag{21}$$

we have

$$\left.\begin{aligned} x_{10}' &= x_1(\mathbf{X}_0, t_0 + \Delta t_1), \\ y_{10}' &= y_1(\mathbf{X}_0, t_0 + \Delta t_1), \\ x_{20}' &= x_2(\mathbf{X}_0, t_0 + \Delta t_1), \\ y_{20}' &= m_1 y_2(\mathbf{X}_0, t_0 + \Delta t_1) + n_1 y_3(\mathbf{X}_0, t_0 + \Delta t_1), \\ y_{30}' &= m_2 y_2(\mathbf{X}_0, t_0 + \Delta t_1) + n_2 y_3(\mathbf{X}_0, t_0 + \Delta t_1), \\ t_0' &= t_0 + \Delta t_1. \end{aligned}\right\} \tag{22}$$

Defining $\mathbf{Q}_2 : \mathbf{\Pi}_1 \to \mathbf{\Pi}_0$ (including an impact) and $\mathbf{Q}_2(\mathbf{X}_1) = \mathbf{X}_1'$, where

$$\left.\begin{aligned} \mathbf{X}_1 &= (x_{11}, y_{11}, x_{21}, y_{21}, y_{31}, t_1) \in \mathbf{\Pi}_1, \\ \mathbf{X}_1' &= (x_{11}', y_{11}', x_{21}', y_{21}', y_{31}', t_1') \in \mathbf{\Pi}_0, \end{aligned}\right\} \tag{23}$$

we have

$$\left.\begin{aligned} x_{11}' &= x_1(\mathbf{X}_1, t_1 + \Delta t_2), \\ y_{11}' &= y_1(\mathbf{X}_1, t_1 + \Delta t_2), \\ x_{21}' &= x_2(\mathbf{X}_1, t_1 + \Delta t_2), \\ y_{21}' &= m_1 y_2(\mathbf{X}_1, t_1 + \Delta t_2) + n_1 y_3(\mathbf{X}_1, t_1 + \Delta t_2), \\ y_{31}' &= m_2 y_2(\mathbf{X}_1, t_1 + \Delta t_2) + n_2 y_3(\mathbf{X}_1, t_1 + \Delta t_2), \\ t_1' &= t_1 + \Delta t_2. \end{aligned}\right\} \tag{24}$$

Thus, as shown in Fig. 2, the Poincaré map of the vibro-impact system can be established as

$$\mathbf{P} = \mathbf{Q}_2 \circ \mathbf{Q}_1, \quad \mathbf{P} : \mathbf{\Pi}_0 \mapsto \mathbf{\Pi}_0. \tag{25}$$

Lemma 4. (*Yue and Xie* [28]). *The Poincaré map of the 3-dof vibro-impact system has the symmetry property*:

$$\mathbf{R} \circ \mathbf{Q_1} = \mathbf{Q_2} \circ \mathbf{R}. \tag{26}$$

Proof. According to Eq. (20), and considering $\Delta t_1 = \Delta t_2$, for $\mathbf{X}_0 \in \mathbf{\Pi}_1$, we have

$$\begin{aligned}\mathbf{R} \circ \mathbf{Q}_1(\mathbf{X}_0) &= \mathbf{R}(x_1(\mathbf{X}_0, t_0 + \Delta t_1), y_1(\mathbf{X}_0, t_0 + \Delta t_1), x_2(\mathbf{X}_0, t_0 + \Delta t_1), m_1 y_2(\mathbf{X}_0, t_0 + \Delta t_1) \\ &\quad + n_1 y_3(\mathbf{X}_0, t_0 + \Delta t_1), m_2 y_2(\mathbf{X}_0, t_0 + \Delta t_1) + n_2 y_3(\mathbf{X}_0, t_0 + \Delta t_1), t_0 + \Delta t_1) \\ &= (x_1(\mathbf{X}_1, t_1 + \Delta t_1), y_1(\mathbf{X}_1, t_1 + \Delta t_1), x_2(\mathbf{X}_1, t_1 + \Delta t_1), m_1 y_2(\mathbf{X}_1, t_1 + \Delta t_1) \\ &\quad + n_1 y_3(\mathbf{X}_1, t_1 + \Delta t_1), m_2 y_2(\mathbf{X}_1, t_1 + \Delta t_1) + n_2 y_3(\mathbf{X}_1, t_1 + \Delta t_1), t_1 + \Delta t_1) \\ &= (x'_{11}, y'_{11}, x'_{21}, y'_{21}, y'_{31}, t'_1) \\ &= \mathbf{X}'_1.\end{aligned} \tag{27}$$

However, as shown in Fig. 2,

$$\mathbf{Q}_2\mathbf{R}(\mathbf{X}_0) = \mathbf{Q}_2(\mathbf{X}_1) = \mathbf{X}'_1, \tag{28}$$

such that Eq. (26) is proved.

Eq. (26) can be rewritten as

$$\mathbf{Q_2} = \mathbf{R} \circ \mathbf{Q_1} \circ \mathbf{R}^{-1}. \tag{29}$$

Introducing a map

$$\mathbf{Q}_\gamma = \mathbf{R}^{-1} \circ \mathbf{Q}_1, \tag{30}$$

we obtain the Poincaré map as below:

$$\mathbf{P} = \mathbf{Q}_2 \circ \mathbf{Q}_1 = \mathbf{R} \circ \mathbf{Q}_1 \circ \mathbf{R}^{-1} \circ \mathbf{Q}_1 = \mathbf{R}^2 \circ (\mathbf{R}^{-1} \circ \mathbf{Q}_1)^2 = \mathbf{Q}_\gamma^2. \tag{31}$$

That is, the Poincaré map $\mathbf{P}$ is the second iteration of $\mathbf{Q}_\gamma$, where $\mathbf{Q}_\gamma$ has no symmetry. Clearly, Eq. (31) implies the symmetry property of the Poincaré map of the vibro-impact system. It should be mentioned that since Δt_1 and Δt_2 are determined by equations $x_2 - x_3 = +h$ and $x_2 - x_3 = -h$ implicitly, $\mathbf{Q}_1$,$\mathbf{Q}_2$, $\mathbf{Q}_\gamma$ and $\mathbf{P}$ are all implicit maps. □

5. Effect of the symmetry of the Poincaré map on possible bifurcations

If $\mathbf{X}_0 \in \mathbf{\Pi}_0$ satisfies $\mathbf{P}(\mathbf{X}_0) = \mathbf{X}_0$, then $\mathbf{X}_0$ is a fixed point of the Poincaré map $\mathbf{P}$, corresponding to the associated periodic motion of the system.

Definition 5. (Symmetric fixed point). If the fixed point $\mathbf{X}_0$ satisfies

$$\mathbf{X}_0 = \mathbf{Q}_\gamma(\mathbf{X}_0), \tag{32}$$

then $\mathbf{X}_0$ is said to be a symmetric fixed point (or symmetric period n–2 fixed point) of the Poincaré map $\mathbf{P}$, corresponding to the associated symmetric period n–2 motion of the system.

Since the symmetric period n–2 motion of the vibro-impact system corresponds to the symmetric fixed point of the Poincaré map, we can investigate bifurcations of the symmetric period n–2 motion by researching into bifurcations of the associated symmetric fixed point. The eigenvalues of the Jacobi matrix $\mathbf{DP}(\mathbf{X}_0)$ determine the stability of the symmetric fixed point $\mathbf{X}_0$ of the Poincaré map. Suppose that all the eigenvalues of $\mathbf{DP}(\mathbf{X}_0)$ lie inside the unit circle, the symmetric fixed point $\mathbf{X}_0$ is stable. If there are some eigenvalues crossing the unit circle, various bifurcations take place [29]. When there is a real eigenvalue crossing the unit circle at $+1$, the symmetric fixed point changes its stability, and bifurcates into a pair of antisymmetric fixed points which have the same stability via pitchfork bifurcation [28]. If there is a pair of complex conjugate eigenvalues and a real eigenvalue -1 crossing the unit circle simultaneously, Hopf–flip bifurcation occurs. If there are two pairs of complex conjugate eigenvalues escaping from the unit circle simultaneously, Hopf–Hopf bifurcation takes place.

The method of computing $\mathbf{DP}(\mathbf{X}_0)$ is similar to that shown in Ref. [28]. The Poincaré map $\mathbf{P}$ is a composition of following four sub-maps: (I) $\mathbf{P}_1$: The map from the instant after impacting at the right stop ($t = t_0$) to the instant before impacting at the left stop ($t = t_1$); (II) $\mathbf{P}_2$: The map of impacting at the left stop ($t = t_1$); (III) $\mathbf{P}_3$: The map from the instant after impacting at the left stop ($t = t_1$) to the instant before impacting at the right stop ($t = t_2$); (IV) $\mathbf{P}_4$: The map of impacting at the right stop ($t = t_2$). Hence, the Poincaré map can be expressed as: $\mathbf{P} = \mathbf{P}_4 \circ \mathbf{P}_3 \circ \mathbf{P}_2 \circ \mathbf{P}_1$, and its Jacobi matrix can be computed as: $\mathbf{DP} = \mathbf{DP}_4\mathbf{DP}_3\mathbf{DP}_2\mathbf{DP}_1$, where $\mathbf{DP}_i$ is the linearized matrix of sub-maps $\mathbf{P}_i$. Let $\mathbf{DP}_1 = [d_{ij}]_{6\times6}$, we show the entries of the matrix $\mathbf{DP}_1$ in Appendix C. It should be mentioned that since $\mathbf{P}$ is an implicit map, the Jacobi matrix $\mathbf{DP}(\mathbf{X}_0)$ is calculated according to implicit function theorem.

Theorem 6. *For the symmetric fixed point, or the symmetric period n–2 motion, the symmetry property of the Poincaré map suppresses not only codimension-1 period-doubling bifurcation, but also Hopf–flip bifurcation and pitchfork–flip bifurcation completely.*

Proof. Let $\mathbf{DP}$ and $\mathbf{DQ}_\gamma$ be the Jacobian matrices of $\mathbf{P}$ and $\mathbf{Q}_\gamma$ evaluated at the symmetric fixed point $\mathbf{X}_0$, respectively. Then Eq. (31) implies

$$\mathbf{DP} = (\mathbf{DQ}_\gamma)^2. \tag{33}$$

First we consider codimension-1 bifurcation of $\mathbf{X}_0$. If and only if $\mathbf{DQ}_\gamma$ has a simple real eigenvalue $\tilde{\lambda}$, the Jacobian matrix $\mathbf{DP}$ has a simple real eigenvalue $\lambda = \tilde{\lambda}^2 > 0$. Therefore, -1 cannot be the eigenvalue of $\mathbf{DP}$, which implies that period-doubling bifurcation cannot occur. That is, the symmetry of the Poincaré map suppresses codimension-1 period-doubling bifurcation. Second, let us discuss codimension-2 bifurcations of the symmetric fixed point $\mathbf{X}_0$. Since $\mathbf{DP}$ cannot have single real eigenvalue -1, the symmetric fixed point $\mathbf{X}_0$ cannot have Hopf–flip bifurcation and pitchfork–flip bifurcation. Here it should be noted that $\mathbf{DP}$ may have a double real eigenvalue -1. □

To sum up, for the symmetric fixed point, or the symmetric period n–2 motion, the symmetry of the Poincaré map suppresses codimension-1 period-doubling bifurcation, Hopf–flip bifurcation and pitchfork–flip bifurcation completely, which gives Theorem 7.

6. Normal forms near two kinds of codimension-two bifurcation points

For the symmetric vibro-impact system with given parameters, let $\lambda = \mathrm{e}^{\pm i\theta} = \cos\theta \pm i\sin\theta$ be the eigenvalue of $\mathbf{DP}$, and $\tilde{\lambda} = \mathrm{e}^{\pm i\tilde{\theta}} = \cos\tilde{\theta} \pm i\sin\tilde{\theta}$ be the eigenvalue of $\mathbf{DQ}_\gamma$, where the angle θ (or $\tilde{\theta}$) denotes the azimuth that λ (or $\tilde{\lambda}$) crosses the unit circle. Since $\mathbf{DP} = (\mathbf{DQ}_\gamma)^2$, we have

$$\lambda = \tilde{\lambda}^2, \tag{34}$$

and

$$\theta = 2\tilde{\theta}. \tag{35}$$

Now we discuss as follows. (I) If $\mathbf{Q}_\gamma$ has a pair of complex conjugate eigenvalues escaping from the unit circle, then $\mathbf{P}$ has also a pair of complex conjugate eigenvalues escaping from the unit circle, and vise versa. Hence, in general case (that is, $\mathbf{P}$ and $\mathbf{Q}_\gamma$ satisfy nonresonant conditions at the same time), codimension one Hopf bifurcation of $\mathbf{Q}_\gamma$ corresponds to codimension one Hopf bifurcation of $\mathbf{P}$, and Hopf–Hopf bifurcation of $\mathbf{Q}_\gamma$ corresponds to Hopf–Hopf bifurcation of $\mathbf{P}$. (II) If $\mathbf{Q}_\gamma$ has a real eigenvalue crossing the unit circle from the point (–1,0) (i.e., $\tilde{\theta} = \pi$), then $\mathbf{P}$ has a real eigenvalue crossing the unit circle from the point (+1,0) (i.e., $\theta = 2\pi$), and vise versa. Therefore, codimension one period-doubling bifurcation of $\mathbf{Q}_\gamma$ corresponds to codimension one pitchfork bifurcation of $\mathbf{P}$, and Hopf–flip bifurcation of $\mathbf{Q}_\gamma$ corresponds to Hopf–pitchfork bifurcation of $\mathbf{P}$. (III) If $\mathbf{Q}_\gamma$ has a pairs of complex conjugate eigenvalues crossing the unit circle near the point (0,i) (i.e., $\tilde{\theta} \approx \pi/2$), then $\mathbf{P}$ has a pairs of complex conjugate eigenvalues crossing the unit circle near the point (–1,0) (i.e., $\theta \approx \pi$), and vise versa. Thus, Hopf bifurcation of $\mathbf{Q}_\gamma$ satisfying 1:4 resonant conditions corresponds to Hopf bifurcation of $\mathbf{P}$ satisfying 1:2 resonant conditions. The contrast of possible bifurcation between the map $\mathbf{P}$ and the map $\mathbf{Q}_\gamma$ is listed in Table 1.

Table 1
The contrast of bifurcation types between the map **P** and the map $\mathbf{Q}_\gamma$.

The map $\mathbf{Q}_\gamma$	The map **P**
General Hopf bifurcation	General Hopf bifurcation
Period-doubling bifurcation	Pitchfork bifurcation
Hopf–Hopf bifurcation	Hopf–Hopf bifurcation
Hopf–flip bifurcation	Hopf–pitchfork bifurcation
Hopf bifurcation satisfying 1:4 resonant conditions	Hopf bifurcation satisfying 1:2 resonant conditions

In this section, we consider Hopf–Hopf bifurcation and Hopf bifurcation satisfying 1:2 resonant conditions of the map **P**. Let the bifurcation parameters be $(\mu_1, \mu_2)^{\mathrm{T}} = \mu$. For some neighborhood of the critical point $\mu_c = (\mu_{1c}, \mu_{2c})^{\mathrm{T}}$, assume that the symmetric fixed point of the map **P** is $\mathbf{X}_0 = (x_{10}, y_{10}, x_{20}, y_{20}, y_{30}, \tau_0)^{\mathrm{T}}$. If the coordinates origin is transferred to this symmetric fixed point, then the symmetric fixed point is $(0,0,0,0,0,0)^{\mathrm{T}} = \mathbf{0}$. Adding a initial perturbation $\Delta\mathbf{X} = (\Delta x_{10}, \Delta y_{10}, \Delta x_{20}, \Delta y_{20}, \Delta y_{30}, \Delta\tau_0)^{\mathrm{T}}$ to this symmetric fixed point, the perturbed map of **P** is

$$\Delta\mathbf{X}' = \mathbf{P}(\Delta\mathbf{X}), \tag{36}$$

Under this coordinates transformation, $(0,0,0,0,0,0)^{\mathrm{T}} = \mathbf{0}$ is also the symmetric fixed point of the map $\mathbf{Q}_\gamma$, and the perturbed map of $\mathbf{Q}_\gamma$ is

$$\Delta\mathbf{X}' = \mathbf{Q}_\gamma(\Delta\mathbf{X}), \tag{37}$$

The following analysis is based on the above two perturbed maps. For convenience, Eqs. (36) and (37) are still written as $\mathbf{X}' = \mathbf{P}(\mathbf{X})$ and $\mathbf{X}' = \mathbf{Q}_\gamma(\mathbf{X})$, respectively. The method of establishing the perturbed map in vibro-impact system is referred to Ref. [13].

6.1. Hopf–Hopf bifurcation

Since Hopf–Hopf bifurcation of $\mathbf{Q}_\gamma$ corresponds to that of **P**, then firstly we consider the normal form of the map $\mathbf{Q}_\gamma$ near Hopf–Hopf bifurcation point. If the Jacobi matrix $\mathbf{DQ}_\gamma(\mu, \mathbf{0})$ of $\mathbf{Q}_\gamma$ at $\mu = \mu_c$ satisfy

(C.1) $\mathbf{DQ}_\gamma(\mu, \mathbf{0})$ has two pairs of complex conjugate eigenvalues on the unit circle: $\tilde{\lambda}_0, \overline{\tilde{\lambda}}_0 = \mathrm{e}^{\pm\mathrm{i}\tilde{\theta}_0}$, $\tilde{\lambda}_1, \overline{\tilde{\lambda}}_1 = \mathrm{e}^{\pm\mathrm{i}\tilde{\theta}_1}$, and all other eigenvalues of $\mathbf{DQ}_\gamma(\mu, \mathbf{0})$ lie in the unit circle;

(C.2) Degenerate eigenvalues λ_0 and λ_1 satisfy non-resonant conditions: $m_0\tilde{\theta}_0/2\pi + m_1\tilde{\theta}_1/2\pi \in \mathbf{Z}$ and have no solution for $|m_1| + |m_2| < N$, where $m_0, m_1 \in \mathbf{Z}$, and N is a sufficiently large integer, then according to the center manifold and the normal form methods, the normal form of the map $\mathbf{Q}_\gamma$ can be given as [25,26]

$$z_0' = \tilde{\lambda}_0 z_0 + \tilde{a}_1 z_0^2 \overline{z}_0 + \tilde{a}_2 z_0 z_1 \overline{z}_1 + O((|z_0| + |z_1|)^5), \tag{38}$$

$$z_1' = \tilde{\lambda}_1 z_1 + \tilde{b}_1 z_0 \overline{z}_0 z_1 + \tilde{b}_2 z_1^2 \overline{z}_1 + O((|z_0| + |z_1|)^5), \tag{39}$$

where the coefficients $\tilde{a}_1$, $\tilde{a}_2$, $\tilde{b}_1$, $\tilde{b}_2$ are shown in Refs. [25,26] in detail. Due to $\mathbf{P} = \mathbf{Q}_\gamma^2$, the normal form of the Poincaré map **P** near Hopf–Hopf bifurcation point is the second iteration of Eqs. (38) and (39), which can be written as

$$z_0' = \lambda_0 z_0 + a_1 z_0^2 \overline{z}_0 + a_2 z_0 z_1 \overline{z}_1 + O((|z_0| + |z_1|)^5), \tag{40}$$

$$z_1' = \lambda_1 z_1 + b_1 z_0 \overline{z}_0 z_1 + b_2 z_1^2 \overline{z}_1 + O((|z_0| + |z_1|)^5), \tag{41}$$

where

$$\lambda_0 = \tilde{\lambda}_0^2, \quad \lambda_1 = \tilde{\lambda}_1^2, \quad a_1' = a_1\tilde{\lambda}_0(1 + \tilde{\lambda}_0\overline{\tilde{\lambda}}_0),$$

$$a_2 = \tilde{a}_2\tilde{\lambda}_0(1 + \tilde{\lambda}_1\overline{\tilde{\lambda}}_1), \quad b_1 = \tilde{b}_1\tilde{\lambda}_1(1 + \tilde{\lambda}_0\overline{\tilde{\lambda}}_0), \quad b_2 = \tilde{b}_2\tilde{\lambda}_1(1 + \tilde{\lambda}_1\overline{\tilde{\lambda}}_1). \tag{42}$$

Eqs. (38)–(42) show that for Hopf–Hopf bifurcation, the normal form of the Poincaré map $\mathbf{P}$ is same to that of the map $\mathbf{Q}_\gamma$, but the coefficients of the associated normal form are different, which will make the different area bound in the two-parameter unfolding portraits near Hopf–Hopf bifurcation.

6.2. Hopf bifurcation in the case of 1:2 resonance

Since Hopf bifurcation of $\mathbf{Q}_\gamma$ satisfying 1:4 resonant conditions corresponds to Hopf bifurcation of $\mathbf{P}$ satisfying 1:2 resonant conditions, then firstly we consider the normal form of Hopf bifurcation of $\mathbf{Q}_\gamma$ satisfying 1:4 resonant conditions. If the Jacobi matrix $\mathbf{DQ}_\gamma(\mu, \mathbf{0})$ of $\mathbf{Q}_\gamma$ at $\mu = \mu_c$ satisfy

(H.1) $\mathbf{DQ}_\gamma(\mu, \mathbf{0})$ has a pairs of complex conjugate eigenvalues on the unit circle: $\tilde{\lambda}_0, \overline{\tilde{\lambda}}_0 = \mathrm{e}^{\pm \mathrm{i}\tilde{\theta}_0}$, and all other eigenvalues of $\mathbf{DQ}_\gamma(\mu, \mathbf{0})$ lie in the unit circle;

(H.2) $\partial\tilde{\lambda}_0(\mu_c)/\partial\mu_1 \neq 0$ and $\partial\tilde{\lambda}_0(\mu_c)/\partial\mu_2 \neq 0$, which is the transversal condition for the two-parameter family;

(H.3) $\tilde{\lambda}_0^4(\mu_c) = 1$ and $\tilde{\lambda}_0(\mu_c) \neq \pm 1$, then the normal form of Hopf bifurcation of $\mathbf{Q}_\gamma$ in 1:4 resonant case can be expressed as [20]

$$\Phi_\mu(z, \bar{z}) = \tilde{\lambda}(\mu)z + \tilde{\alpha}(\mu)z^2\bar{z} + \tilde{\beta}(\mu)\bar{z}^3 + O(|z|^5), \tag{43}$$

where

$$\tilde{\alpha}(0) = \frac{g_{21}}{2} + \frac{|g_{02}|^2}{2(\tilde{\lambda}_0^2 - \overline{\tilde{\lambda}}_0)} + \frac{|g_{11}|^2}{1 - \overline{\tilde{\lambda}}_0} + \frac{g_{11}g_{20}(1 - 2\tilde{\lambda}_0)}{2(\overline{\tilde{\lambda}}_0^2 - \tilde{\lambda}_0)}, \tag{44}$$

$$\tilde{\beta}(0) = \frac{g_{03}}{6} + \frac{g_{02}(g_{11} + 2\bar{g}_{20})}{2(\overline{\tilde{\lambda}}_0^2 - \tilde{\lambda}_0)}, \tag{45}$$

where the coefficients g_{ij} are shown in Ref. [20]. The normal form of the map $\mathbf{P}$ is the second iteration of Eqs. (43), which takes the form

$$\Phi_\mu(z, \bar{z}) = \lambda(\mu)z + \alpha(\mu)z^2\bar{z} + \beta(\mu)\bar{z}^3 + O(|z|^5), \tag{46}$$

where

$$\lambda(\mu) = \tilde{\lambda}^2(\mu), \quad \alpha(\mu) = \tilde{\alpha}(\mu)\tilde{\lambda}(\mu)(1 + \tilde{\lambda}(\mu)\overline{\tilde{\lambda}}(\mu)),$$

$$\beta(\mu) = \tilde{\beta}(\mu)(\tilde{\lambda}(\mu) + \overline{\tilde{\lambda}}^3(\mu)). \tag{47}$$

7. Numerical bifurcation analysis

7.1. Hopf bifurcation of the symmetric fixed point

The vibro-impact system with system parameters (1): $n = 1$, $\zeta = 0.00166$, $\zeta_p = 0.008$, $\omega = 3.88$, $R = 0.8$, $h = 0.08$, $u_{m1} = 0.767$, $u_{m2} = 2$, $u_{k1} = 1$, $u_{k2} = 1$, $u_{f1} = 2$, $u_{f2} = 1$, are considered, and the forcing frequency ω is taken as a control parameter. For $\omega = \omega_{c2} = 2.06777911$, the six eigenvalues of $\mathbf{DP}(\mathbf{X}_0)$ and their moduli can be given as:

$$\lambda_{1,2} = -0.999124 \pm 0.046103i, \quad |\lambda_{1,2}| = 1.000187; \quad \lambda_{3,4} = 0.613510 \pm 0.789685i,$$

$$|\lambda_{3,4}| = 0.999999; \quad \lambda_{5,6} = -0.392817 \pm 0.461321i, \quad |\lambda_{5,6}| = 0.605906.$$

There is a pair of complex conjugate eigenvalues crossing the unit circle, and the remainder of the spectrum of $\mathbf{DP}(\mathbf{X}_0)$ lie inside the unit circle, hence ω_{c2} is the critical value of Hopf bifurcation. As ω increases to $\omega = 2.075$, Hopf bifurcation takes place, and the symmetric fixed point evolves into an invariant circle, see Fig. 3.

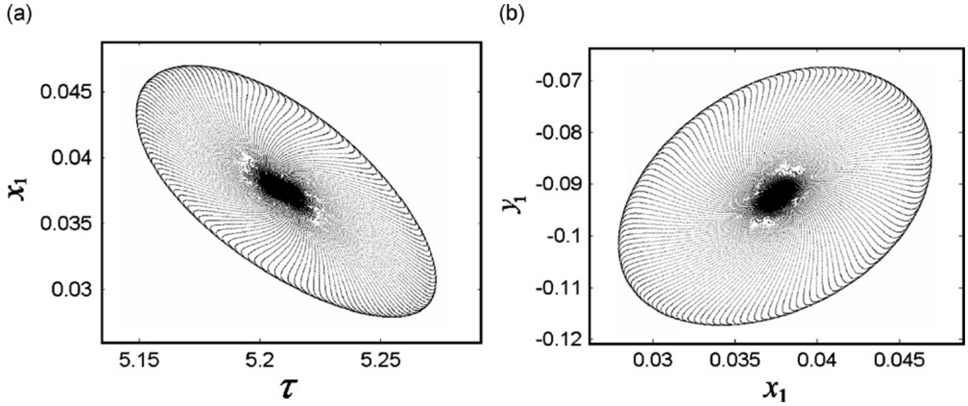

Fig. 3. Phase diagrams in projected Poincaré section: invariant circle bifurcated from the symmetric fixed point via Hopf bifurcation, $\omega = 2.075$, 200 000 iterations. (a): (τ, x_1) plane; (b): (x_1, y_1) plane.

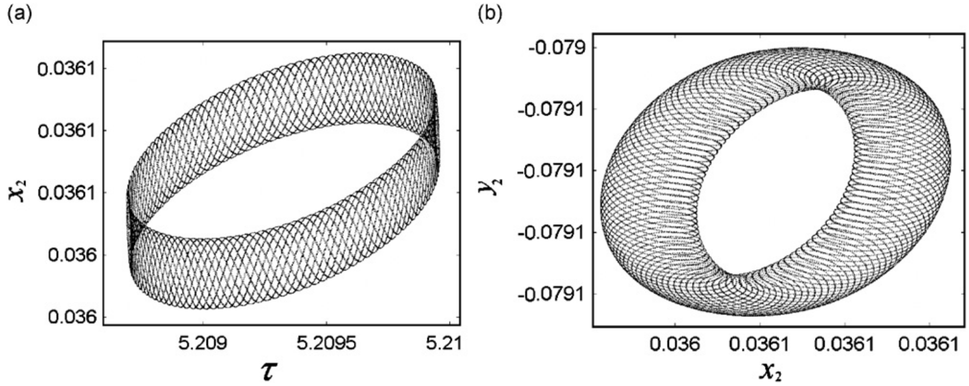

Fig. 4. Phase diagrams in projected Poincaré section: torus $\mathbf{T}^2$ bifurcated from the symmetric fixed point via Hopf–Hopf bifurcation, plotting 50 000 points after 300 000 iterations. (a) (τ, x_2) plane; (b) (x_2, y_2) plane.

7.2. Hopf– Hopf bifurcation of the symmetric fixed point

First we still consider system parameters (1), and choose ζ and u_{m1} as the two control parameters. Changing the values of ζ and u_{m1} simultaneously, we can obtain the critical point of Hopf–Hopf bifurcation. When $\zeta = 0.0016582$ and $u_{m1} = 0.76764$, the six eigenvalues of Jacobi matrix $\mathbf{DP}(\mathbf{X}_0)$ and their moduli can be given as follows:

$$\lambda_{1,2} = 0.61367422 \pm 0.78955938i, \quad |\lambda_{1,2}| = 1.00000004; \quad \lambda_{3,4} = -0.39252793 \pm 0.46175906i,$$

$$|\lambda_{3,4}| = 0.60605248; \quad \lambda_{5,6} = -0.99885430 \pm 0.04785517i, \quad |\lambda_{5,6}| = 1.00000002.$$

There are two pairs of complex conjugate eigenvalues escaping from the unit circle simultaneously. Hence, Hopf–Hopf bifurcation of the symmetric fixed point takes place, and the symmetric fixed point bifurcates into an invariant torus $\mathbf{T}^2$, as shown in Fig. 4.

As the second example, the system parameters (2): $n = 1$, $\zeta_p = 0.002274295$, $R = 0.8$, $h = 0.2$, $u_{m1} = 1.5$, $u_{m2} = 2.8$, $u_{k1} = 1.2$, $u_{k2} = 1$, $u_{f1} = 1.8$, $u_{f2} = 0.6$ are chosen for analysis, and ζ and ω are chosen as the two control parameters. When $\zeta = \zeta_c = 0.012$, $\omega = \omega_c = 2.99793$, the six eigenvalues of Jacobi matrix $\mathbf{DP}(\mathbf{X}_0)$ and their moduli can be given as:

$$\lambda_{1,2} = 0.60621811 \pm 0.79529846i, \quad |\lambda_{1,2}| = 1.00000002; \quad \lambda_{3,4} = -0.94524483 \pm 0.32636215i,$$

$$|\lambda_{3,4}| = 1.00000003; \quad \lambda_{5,6} = -0.38495827 \pm 0.48390611i, \quad |\lambda_{5,6}| = 0.61835103.$$

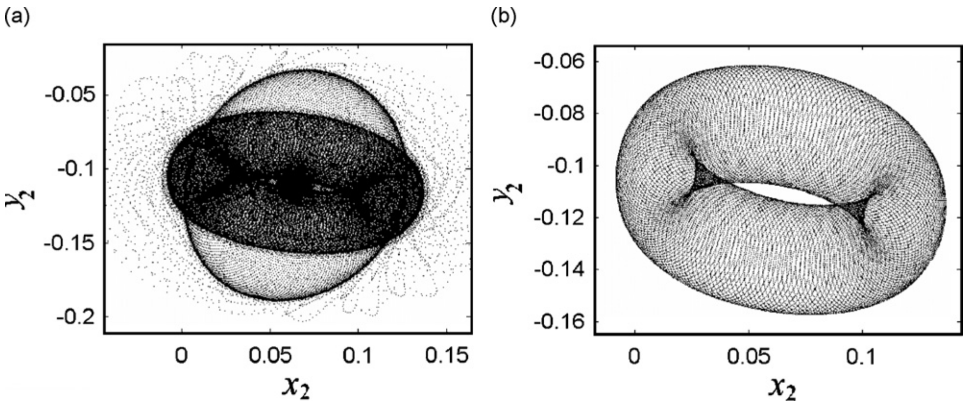

Fig. 5. Phase diagrams in projected Poincaré section: torus $\mathbf{T}^2$ bifurcated from the symmetric fixed point via Hopf–Hopf bifurcation. (a) 600 000 iterations; (b) plotting 100 000 points after 600 000 iterations.

There are two pairs of complex conjugate eigenvalues escaping from the unit circle simultaneously, hence ζ_c and ω_c are the two critical parameter values of Hopf–Hopf bifurcation. When ζ and ω vary near the critical parameter values, invariant torus $\mathbf{T}^2$ can be obtained. For example, when $\zeta = \zeta_c - 0.00008$ and $\omega = \omega_c - 0.001$, there is an invariant torus $\mathbf{T}^2$ bifurcated from the symmetric fixed point, as shown in Fig. 5.

7.3. Hopf bifurcation in 1:2 resonant case

Now we consider system parameters (3): $n = 1$, $\zeta_p = 0.005$, $R = 0.8$, $h = 0.05$, $u_{m1} = 0.6$, $u_{m2} = 3$, $u_{k1} = 0.8$, $u_{k2} = 1.5$, $u_{f1} = 1$, $u_{f2} = 2$, and ζ and ω are taken as two bifurcation parameters. With $\zeta = 0.015$ and $\omega = 3.38$, the six eigenvalues of Jacobi matrix $\mathbf{DP}(\mathbf{X}_0)$ and their moduli are

$$\lambda_{1,2} = -1.0098 \pm 0.0120i, \quad |\lambda_{1,2}| = 1.0099; \quad \lambda_{3,4} = 0.4919 \pm 0.8659i,$$

$$|\lambda_{3,4}| = 0.9959; \quad \lambda_{5,6} = -0.5156 \pm 0.3093i, \quad |\lambda_{5,6}| = 0.6013.$$

there are a pair of conjugate complex eigenvalues $\lambda_{1,2}$ escaping the unit circle near the point $(-1,0)$, hence the iteration of $\mathbf{P}$ will exhibit the characteristic of 1:2 resonance. With small perturbation, the unstable symmetric fixed point bifurcates into a circle from two directions, as shown in Fig. 6(a). However, for the map $\mathbf{Q}_\gamma$, the 1:4 resonant condition is satisfied, and the unstable symmetric fixed point bifurcates into the same circle from four directions, as shown in Fig. 6(b). It is interesting that the Hopf circle in Fig. 6(a) and (b) is unstable, and will evolve into torus $\mathbf{T}^2$ finally with increasing iteration number, as shown in Fig. 6(c) and (d). It is clear that the evolvement sequence is: unstable symmetric fixed point$\rightarrow$unstable circle$\rightarrow$stable torus $\mathbf{T}^2$. Here the original purpose of our study is aimed at the 1:2 resonance of the map $\mathbf{P}$, but the phase portrait in projected Poincare section exhibits both the characteristic of 1:2 resonance and that of torus $\mathbf{T}^2$. The reason for this is that there are another pair of conjugate complex eigenvalues $\lambda_{3,4}$ close to the unit circle. At the same time, the phase portrait of the map $\mathbf{Q}_\gamma$ exhibits both the characteristic of 1:4 resonance and that of torus $\mathbf{T}^2$, as shown in Fig. 6(d). Fig. 6(e) and (f) represent the final stable torus of the map $\mathbf{P}$ and $\mathbf{Q}_\gamma$, respectively. It is shown that the curve density on the torus of the map $\mathbf{Q}_\gamma$ is double of that on the torus of the map $\mathbf{P}$, which is caused by $\mathbf{P} = \mathbf{Q}_\gamma^2$ and $\mathbf{Q}_\gamma(\mathbf{X}) \neq \mathbf{X}$.

With $\zeta = 0.007$ and $\omega = 3.365$, two stable isolated circles appear in the Poincaré section of the map $\mathbf{P}$, which reflects also the characteristic of 1:2 resonance of the map $\mathbf{P}$, as shown in Fig. 7(a) and (b). The evolvement sequence is: an unstable symmetric fixed point$\rightarrow$an unstable circle$\rightarrow$two stable isolated circles, and the two stable isolated circles correspond to $2 \times \mathbf{T}^1$ torus in phase space. However, for the map $\mathbf{Q}_\gamma$, four isolated circles appear, which reflects the characteristic of 1:4 resonance of the map $\mathbf{Q}_\gamma$, as shown in Fig. 7(c) and (d). The evolvement sequence is: an unstable symmetric fixed point$\rightarrow$an unstable circle$\rightarrow$four stable isolated circles, and the four stable isolated circles correspond to $4 \times \mathbf{T}^1$ torus in phase space.

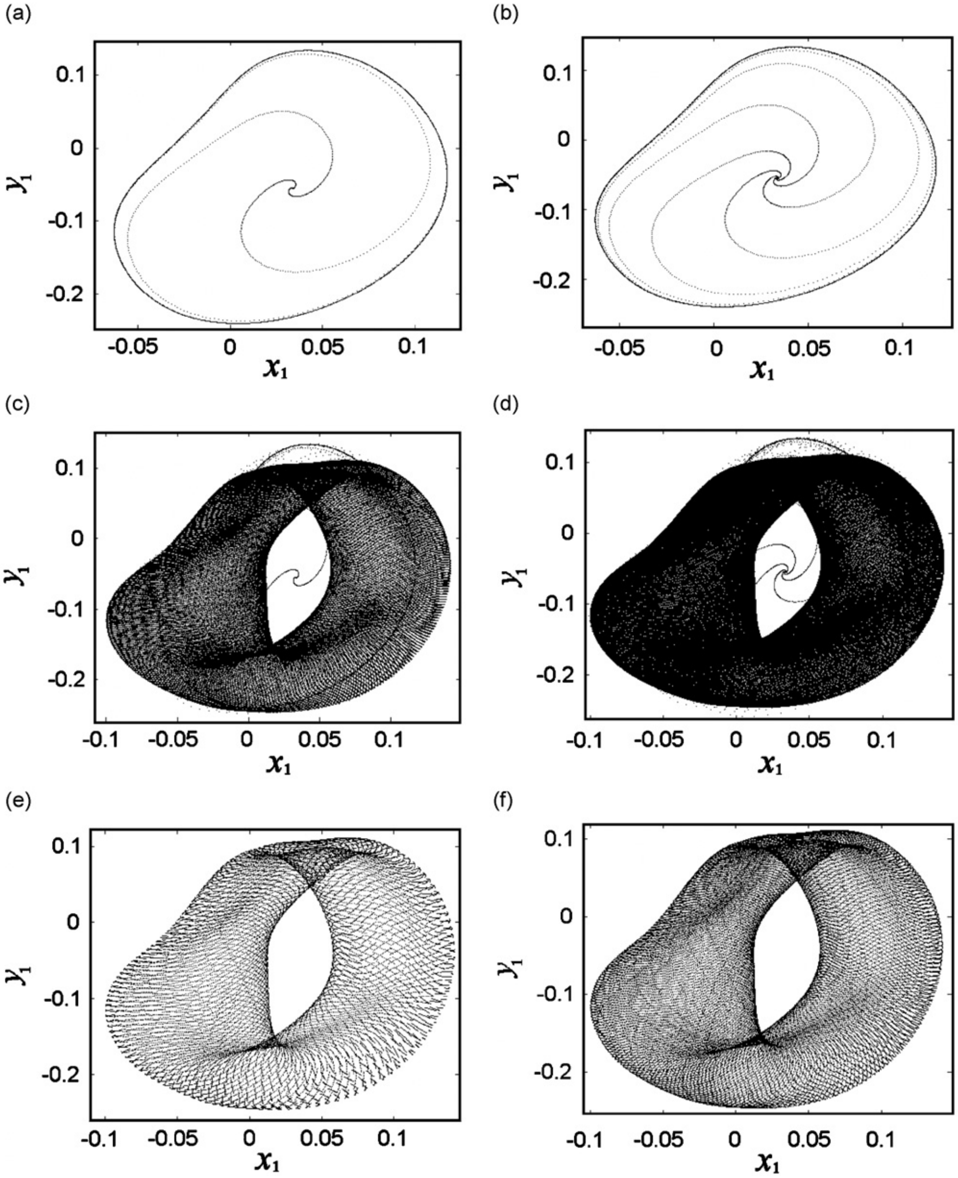

Fig. 6. Phase diagrams in projected Poincaré section: coexistence of an unstable circle and a stable torus: (a), (c) and (e), the map **P**, where (a) 7500 iterations, (c) 150 000 iterations, (e) plotting 20 000 points after 150 000 iterations; (b), (d) and (f), the map $\mathbf{Q}_\gamma$, where (b) 15 000 iterations, (d) 300 000 iterations, (f) plotting 40 000 points after 300 000 iterations.

8. Conclusions

For the three-degree-of-freedom (3-dof), vibro-impact system with symmetric two-sided constraints, it is certain that the Poincaré map has some symmetry property, which suppresses period-doubling bifurcation, Hopf–flip bifurcation and pitchfork–flip bifurcation of the symmetric period n–2 motion.

Due to the symmetric property, the Poincaré map **P** can be expressed as the second iteration of another implicit map $\mathbf{Q}_\gamma$, and $\mathbf{Q}_\gamma$ has no symmetry. Consequently, Hopf–Hopf bifurcation and Hopf bifurcation satisfying 1:2 resonance conditions of the Poincaré map **P** correspond to Hopf–Hopf bifurcation and Hopf bifurcation satisfying 1:4 resonance conditions of the map $\mathbf{Q}_\gamma$, respectively. It is shown that for the corresponding codimension two bifurcation, the normal form of the Poincaré map **P** are same to that of the map $\mathbf{Q}_\gamma$, but the coefficients of the normal map are different. Since **P** is a composition of four sub-maps and

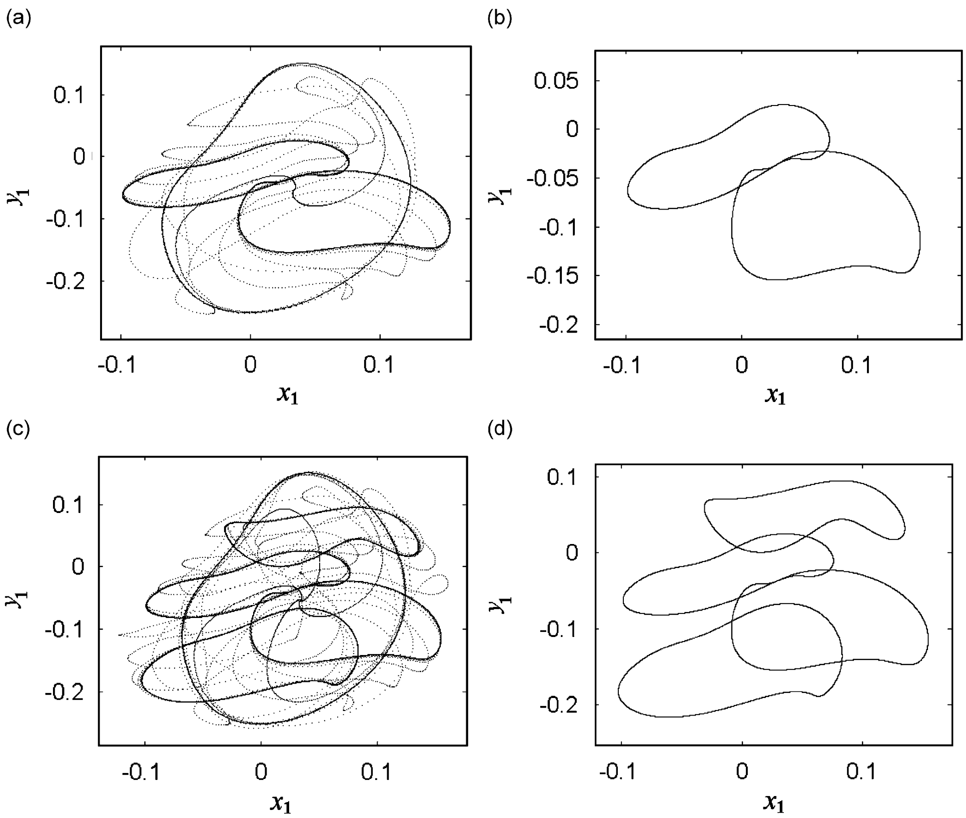

Fig. 7. Phase diagrams in projected Poincaré section: two stable isolated circles for the map **P** and four stable isolated circles for the map $\mathbf{Q}_\gamma$. (a) **P**, 60 000 iterations; (b) **P**, plotting 30 000 points after 60 000 iterations; (c) $\mathbf{Q}_\gamma$, 60 000 iterations; (d) $\mathbf{Q}_\gamma$, plotting 30 000 points after 60 000 iterations.

$\mathbf{Q}_\gamma$ is a composition of two sub-maps, the method of computing the normal forms of **P** via $\mathbf{Q}_\gamma$ is more brief than that via **P** itself.

Under some parameter combination, the Poincaré map **P** of the system can exhibit both the characteristic of 1:2 resonance and that of torus $\mathbf{T}^2$. The reason for this is that there are a pair of conjugate complex eigenvalues escaping from the unit circle near the point $(-1,0)$ and another pair of conjugate complex eigenvalues close to the unit circle at the same time. By numerical simulations, we also obtain $2\times\mathbf{T}^1$ torus of map **P**, which corresponds to $4\times\mathbf{T}^1$ torus of map $\mathbf{Q}_\gamma$.

The vibro-impact system with symmetric constraints considered in the paper has characteristics as follows: (a) the coefficient of restitution at the right stop is same to that at the left stop; (b) between any two consecutive impacts, the non-dimensional vibration equation $\dot{\mathbf{X}} = \mathbf{F}(\mathbf{X}, t)$ satisfy $\mathbf{F}(\mathbf{X}, t) = \mathbf{F}(\mathbf{X}, t + (2\pi/\omega))$ and $\mathbf{F}(\mathbf{X}, t) = -\mathbf{F}(-\mathbf{X}, t + (\pi/\omega))$ (i.e., Eqs. (12) and (13) stand), where ω denotes the non-dimensional excitation frequency. If only the above two conditions are satisfied, the methods presented in Section 4 can be applied to other multi-degree-of-freedom vibro-impact systems with two-sided constraints. Hence, the symmetry of Poincaré map can be deduced subsequently, and the other conclusions presented in this paper are also effective for this kind of vibro-impact systems with symmetric two-sided constraints. This kind of vibro-impact systems is also called *symmetric* vibro-impact system in our studies.

Acknowledgments

This work is supported by National Natural Science Foundation of China (10772151, 10472096) and Scientific Research Project for Young Teacher by Southwest Jiaotong University (2008Q059) and Fund from Doctoral innovation of Southwest Jiaotong University.

Appendix A. The phase angle and the integration constants

$$\tau_0 = \begin{cases} 2\tan^{-1}\left(\dfrac{S_{mn} \pm \sqrt{S_{mn}^2 + C_{mn}^2 - h_{mn}^2}}{C_{mn} - h_{mn}}\right), & h_{mn} \neq C_{mn}; \\ 2\tan^{-1}\left(-\dfrac{h_{mn} + C_{mn}}{2S_{mn}}\right), & h_{mn} = C_{mn}; \end{cases} \tag{A.1}$$

$$a_1 = \frac{-m_c \cos\tau_0 - m_s \sin\tau_0 - m_h}{m_a}, \tag{A.2}$$

$$a_2 = \frac{|U|}{|G|} a_1, \tag{A.3}$$

$$a_3 = p_{o4} a_1 + d_{o4} \cos\tau_0 + f_{o4} \sin\tau_0 + \frac{h}{o_4}, \tag{A.4}$$

$$b_1 = \frac{|Q|}{|G|} a_1, \tag{A.5}$$

$$b_2 = \frac{|V|}{|G|} a_1, \tag{A.6}$$

$$b_3 = p_{og3} a_1 + d_{og3} \cos\tau_0 + f_{og3} \sin\tau_0 + h_3, \tag{A.7}$$

where

$$C_{mn} = m_c n_a - n_c m_a, \quad S_{mn} = m_s n_a - n_s m_a, \quad h_{mn} = m_h n_a - n_h m_a, \tag{A.8}$$

$$m_a = p_6 + q_6 q_g + u_6 u_g + v_6 v_g + o_6 p_{o4} + g_6 p_{og3},$$

$$m_c = o_6 d_{o4} + g_6 d_{og3} + d_6, \quad m_s = o_6 f_{o4} + g_6 d_{og3} + f_6, \quad m_h = \frac{o_6 h}{o_4} + g_6 h_3 \tag{A.9}$$

$$n_a = p_7 + q_7 q_g + u_7 u_g + v_7 v_g + o_7 p_{o4} + g_7 p_{og3},$$

$$n_c = o_7 d_{o4} + g_7 d_{og3} + d_7, \quad n_s = o_7 f_{o4} + g_7 d_{og3} + f_7, \quad m_h = \frac{o_7 h}{o_4} + g_7 h_3, \tag{A.10}$$

$$G = \begin{bmatrix} q_1 & u_1 & v_1 \\ q_2 & u_2 & v_2 \\ q_5 & u_5 & v_5 \end{bmatrix},$$

$$Q = \begin{bmatrix} -p_1 & u_1 & v_1 \\ -p_2 & u_2 & v_2 \\ -p_5 & u_5 & v_5 \end{bmatrix}, \quad U = \begin{bmatrix} q_1 & -p_1 & v_1 \\ q_2 & -p_2 & v_2 \\ q_5 & -p_5 & v_5 \end{bmatrix}, \quad V = \begin{bmatrix} q_1 & u_1 & -p_1 \\ q_2 & u_2 & -p_2 \\ q_5 & u_5 & -p_5 \end{bmatrix}, \tag{A.11}$$

$$p_{o4} = -\frac{p_4 + u_4 u_g}{o_4}, \quad d_{o4} = -\frac{d_4}{o_4}, \quad f_{o4} = -\frac{f_4}{o_4}, \tag{A.12}$$

$$p_{og3} = -\frac{o_3}{g_3} p_{o4}, \quad d_{og3} = -\frac{o_3}{g_3} d_{o4}, \quad f_{og3} = -\frac{o_3}{g_3} f_{o4}, \quad h_3 = -\frac{o_3}{o_4 g_3} h, \tag{A.13}$$

where

$$p_1 = \psi_{11}(1 + e_1 \cos(\omega_{d1}t_1)), \quad q_1 = \psi_{11}e_1 \sin(\omega_{d1}t_1),$$

$$u_1 = \psi_{12}(1 + e_2 \cos(\omega_{d2}t_1)), \quad v_1 = \psi_{12}e_2 \sin(\omega_{d2}t_1), \tag{A.14}$$

$$p_2 = \psi_{21}(1 + e_1 \cos(\omega_{d1}t_1)), \quad q_2 = \psi_{21}e_1 \sin(\omega_{d1}t_1),$$

$$u_2 = \psi_{22}(1 + e_2 \cos(\omega_{d2}t_1)), \quad v_2 = \psi_{22}e_2 \sin(\omega_{d2}t_1), \tag{A.15}$$

$$o_3 = 1 + e_3 \cos(\omega_{d3}t_1), \quad g_3 = e_3 \sin(\omega_{d3}t_1), \tag{A.16}$$

$$p_4 = \psi_{21}, \quad u_4 = \psi_{22}, \quad o_4 = -1, \quad f_4 = \psi_{21}A_1 + \psi_{22}A_2 - A_3, \quad d_4 = \psi_{21}B_1 + \psi_{22}B_2 - B_3, \tag{A.17}$$

$$p_5 = \psi_{11}\eta_1 + \psi_{11}e_1(\eta_1 \cos(\omega_{d1}t_1) + \omega_{d1} \sin(\omega_{d1}t_1)),$$

$$q_5 = -\psi_{11}\omega_{d1} - \psi_{11}e_1(\omega_{d1} \cos(\omega_{d1}t_1) - \eta_1 \sin(\omega_{d1}t_1)),$$

$$u_5 = \psi_{12}\eta_2 + \psi_{12}e_2(\eta_2 \cos(\omega_{d2}t_1) + \omega_{d2} \sin(\omega_{d2}t_1)),$$

$$v_5 = -\psi_{12}\omega_{d2} - \psi_{12}e_2(\omega_{d2} \cos(\omega_{d2}t_1) - \eta_2 \sin(\omega_{d2}t_1)), \tag{A.18}$$

$$p_6 = \psi_{21}\eta_1 + m_1\psi_{21}e_1(\eta_1 \cos(\omega_{d1}t_1) + \omega_{d1} \sin(\omega_{d1}t_1)),$$

$$q_6 = -\psi_{21}\omega_{d1} - m_1\psi_{21}e_1(\omega_{d1} \cos(\omega_{d1}t_1) - \eta_1 \sin(\omega_{d1}t_1)),$$

$$u_6 = \psi_{22}\eta_2 + m_1\psi_{22}e_2(\eta_2 \cos(\omega_{d2}t_1) + \omega_{d2} \sin(\omega_{d2}t_1)),$$

$$v_6 = -\psi_{22}\omega_{d2} - m_1\psi_{22}e_2(\omega_{d2} \cos(\omega_{d2}t_1) - \eta_2 \sin(\omega_{d2}t_1)),$$

$$o_6 = n_1e_3(\eta_3 \cos(\omega_{d3}t_1) + \omega_{d3} \sin(\omega_{d3}t_1)),$$

$$g_6 = -n_1e_3(\omega_{d3} \cos(\omega_{d3}t_1) - \eta_3 \sin(\omega_{d3}t_1)),$$

$$d_6 = (-\psi_{21}A_1 - \psi_{22}A_2 + m_1\psi_{21}A_1 + m_1\psi_{22}A_2 + n_1A_3)\omega,$$

$$f_6 = (\psi_{21}B_1 + \psi_{22}B_2 - m_1\psi_{21}B_1 - m_1\psi_{22}B_2 - n_1B_3)\omega, \tag{A.19}$$

$$p_7 = m_2\psi_{21}e_1(\eta_1 \cos(\omega_{d1}t_1) + \omega_{d1} \sin(\omega_{d1}t_1)),$$

$$q_7 = -m_2\psi_{21}e_1(\omega_{d1} \cos(\omega_{d1}t_1) - \eta_1 \sin(\omega_{d1}t_1)),$$

$$u_7 = m_2\psi_{22}e_2(\eta_2 \cos(\omega_{d2}t_1) + \omega_{d2} \sin(\omega_{d2}t_1)),$$

$$v_7 = -m_2\psi_{22}e_2(\omega_{d2} \cos(\omega_{d2}t_1) - \eta_2 \sin(\omega_{d2}t_1)),$$

$$o_7 = \eta_3 + n_2e_3(\eta_3 \cos(\omega_{d3}t_1) + \omega_{d3} \sin(\omega_{d3}t_1)),$$

$$g_7 = -\omega_{d3} - n_2e_3(\omega_{d3} \cos(\omega_{d3}t_1) - \eta_3 \sin(\omega_{d3}t_1)),$$

$$d_7 = (-A_3 + m_2\psi_{21}A_1 + m_2\psi_{22}A_2 + n_2A_3)\omega,$$

$$f_7 = (B_3 - m_2\psi_{21}B_1 - m_2\psi_{22}B_2 - n_2B_3)\omega, \tag{A.20}$$

where

$$e_i = e^{-\eta_i t_1}, \quad t_1 = \frac{n\pi}{\omega}. \tag{A.21}$$

Appendix B. The integration constants a_{ij} and b_{ij} determined by the initial conditions after impacting

Let the initial conditions be x_{10}, $\dot{x}_{10}$, x_{20}, $\dot{x}_{20}$, $\dot{x}_{30}$, τ_0, the integration constants a_{ij} and b_{ij} can be expressed as

$$\left.\begin{aligned}
a_{11} &= U_{a1}\sin\tau_0 + V_{a1}\cos\tau_0 + P_{a1}x_{10} + Q_{a1}x_{20},\\
a_{21} &= U_{a2}\sin\tau_0 + V_{a2}\cos\tau_0 + P_{a2}x_{10} + Q_{a2}x_{20},\\
a_{31} &= U_{a3}\sin\tau_0 + V_{a3}\cos\tau_0 + P_{a3}x_{10} + Q_{a3}x_{20} - h,\\
b_{11} &= U_{b1}\sin\tau_0 + V_{b1}\cos\tau_0 + P_{b1}x_{10} + Q_{b1}x_{20} + M_{b1}\dot{x}_{10} + N_{b1}\dot{x}_{20},\\
b_{21} &= U_{b2}\sin\tau_0 + V_{b2}\cos\tau_0 + P_{b2}x_{10} + Q_{b2}x_{20} + M_{b2}\dot{x}_{10} + N_{b2}\dot{x}_{20},\\
b_{31} &= U_{b3}\sin\tau_0 + V_{b3}\cos\tau_0 + P_{b3}x_{10} + Q_{b3}x_{20} + M_{b3}\dot{x}_{30} - \frac{\eta_3 h}{\omega_{d3}},
\end{aligned}\right\} \tag{B.1}$$

$$\left.\begin{aligned}
a_{12} &= U_{a1}\sin\tau_0' + V_{a1}\cos\tau_0' + P_{a1}x_{10}' + Q_{a1}x_{20}',\\
a_{22} &= U_{a2}\sin\tau_0' + V_{a2}\cos\tau_0' + P_{a2}x_{10}' + Q_{a2}x_{20}',\\
a_{32} &= U_{a3}\sin\tau_0' + V_{a3}\cos\tau_0' + P_{a3}x_{10}' + Q_{a3}x_{20}' + h,\\
b_{12} &= U_{b1}\sin\tau_0' + V_{b1}\cos\tau_0' + P_{b1}x_{10}' + Q_{b1}x_{20}' + M_{b1}\dot{x}_{10}' + N_{b1}\dot{x}_{20}',\\
b_{22} &= U_{b2}\sin\tau_0' + V_{b2}\cos\tau_0' + P_{b2}x_{10}' + Q_{b2}x_{20}' + M_{b2}\dot{x}_{10}' + N_{b2}\dot{x}_{20}',\\
b_{32} &= U_{b3}\sin\tau_0' + V_{b3}\cos\tau_0' + P_{b3}x_{10}' + Q_{b3}x_{20}' + M_{b3}\dot{x}_{30}' + \frac{\eta_3 h}{\omega_{d3}},
\end{aligned}\right\} \tag{B.2}$$

where

$$(x_{10}', \dot{x}_{10}', x_{20}', \dot{x}_{20}', \dot{x}_{30}', \tau_0') = (-x_{10}, -\dot{x}_{10}, -x_{20}, -\dot{x}_{20}, -\dot{x}_{30}, \tau_0 + n\pi), \tag{B.3}$$

$$U_{a1} = \frac{u_{sa1}}{|D_a|}, \quad V_{a1} = \frac{v_{ca1}}{|D_a|}, \quad P_{a1} = \frac{\psi_{22}}{|D_a|}, \quad Q_{a1} = -\frac{\psi_{12}}{|D_a|}, \tag{B.4}$$

$$U_{a2} = \frac{u_{sa2}}{|D_a|}, \quad V_{a2} = \frac{v_{ca2}}{|D_a|}, \quad P_{a2} = -\frac{\psi_{21}}{|D_a|}, \quad Q_{a2} = \frac{\psi_{11}}{|D_a|}, \tag{B.5}$$

$$\begin{gathered}
U_{a3} = \psi_{21}U_{a1} + \psi_{21}A_1 + \psi_{22}A_2 - A_3, \quad V_{a3} = \psi_{21}V_{a1} + \psi_{21}B_1 + \psi_{22}B_2 - B_3,\\
P_{a3} = \psi_{21}P_{a1} + \psi_{22}P_{a2}, \quad Q_{a3} = \psi_{21}Q_{a1} + \psi_{22}Q_{a2}
\end{gathered} \tag{B.6}$$

$$U_{b1} = \frac{u_{sb1}}{|D_b|}, \quad V_{b1} = \frac{v_{cb1}}{|D_b|}, \quad P_{b1} = \frac{p_{xb1}}{|D_b|}, \quad Q_{b1} = -\frac{q_{xb1}}{|D_b|}, \quad M_{b1} = \frac{m_{xb1}}{|D_b|}, \quad N_{b1} = \frac{n_{xb1}}{|D_b|}, \tag{B.7}$$

$$U_{b2} = \frac{u_{sb2}}{|D_b|}, \quad V_{b2} = \frac{v_{cb2}}{|D_b|}, \quad P_{b2} = \frac{p_{xb2}}{|D_b|}, \quad Q_{b2} = -\frac{q_{xb2}}{|D_b|}, \quad M_{b2} = \frac{m_{xb2}}{|D_b|}, \quad N_{b2} = \frac{n_{xb2}}{|D_b|}, \tag{B.8}$$

$$U_{b3} = \frac{\eta_3 U_{a3} + B_3\omega}{\omega_{d3}}, \quad V_{b3} = \frac{\eta_3 V_{a3} - A_3\omega}{\omega_{d3}}, \quad P_{b3} = \frac{\eta_3 P_{a3}}{\omega_{d3}}, \quad Q_{b3} = \frac{\eta_3 Q_{a3}}{\omega_{d3}}, \quad M_{b3} = \frac{1}{\omega_{d3}}, \tag{B.9}$$

where

$$D_a = \psi, \quad D_b = \begin{bmatrix} \psi_{11}\omega_{d1} & \psi_{12}\omega_{d2} \\ \psi_{21}\omega_{d1} & \psi_{22}\omega_{d2} \end{bmatrix}, \tag{B.10}$$

$$\begin{aligned}
u_{sa1} &= \psi_{12}(\psi_{21}A_1 + \psi_{22}A_2) - \psi_{22}(\psi_{11}A_1 + \psi_{12}A_2),\\
v_{ca1} &= \psi_{12}(\psi_{21}B_1 + \psi_{22}B_2) - \psi_{22}(\psi_{11}B_1 + \psi_{12}B_2),\\
u_{sa2} &= \psi_{22}(\psi_{11}A_1 + \psi_{12}A_2) - \psi_{11}(\psi_{21}A_1 + \psi_{22}A_2),
\end{aligned} \tag{B.11}$$

$$v_{ca2} = \psi_{21}(\psi_{11}B_1 + \psi_{12}B_2) - \psi_{11}(\psi_{21}B_1 + \psi_{22}B_2), \tag{B.12}$$

$$u_{sb1} = \psi_{22}\omega_{d2}u_{s1} - \psi_{12}\omega_{d2}u_{s2}, \quad v_{cb1} = \psi_{22}\omega_{d2}v_{s1} - \psi_{12}\omega_{d2}v_{s2},$$

$$p_{xb1} = \psi_{22}\omega_{d2}p_{s1} - \psi_{12}\omega_{d2}p_{s2}, \quad q_{xb1} = \psi_{22}\omega_{d2}q_{s1} - \psi_{12}\omega_{d2}q_{s2},$$

$$m_{xb1} = \psi_{22}\omega_{d2}, \quad n_{xb1} = -\psi_{12}\omega_{d2}, \tag{B.13}$$

$$u_{sb2} = \psi_{11}\omega_{d1}u_{s2} - \psi_{21}\omega_{d1}u_{s1}, \quad v_{cb2} = \psi_{11}\omega_{d1}v_{s2} - \psi_{21}\omega_{d1}v_{s1},$$

$$p_{xb2} = \psi_{11}\omega_{d1}p_{s2} - \psi_{21}\omega_{d1}p_{s1}, \quad q_{xb2} = \psi_{11}\omega_{d1}q_{s2} - \psi_{21}\omega_{d1}q_{s1},$$

$$m_{xb2} = -\psi_{21}\omega_{d1}, \quad n_{xb2} = \psi_{11}\omega_{d1}, \tag{B.14}$$

where

$$u_{s1} = \psi_{11}\eta_1 U_{a1} + \psi_{12}\eta_2 U_{a2} + \psi_{11}B_1\omega + \psi_{12}B_2\omega,$$

$$v_{s1} = \psi_{11}\eta_1 V_{a1} + \psi_{12}\eta_2 V_{a2} - \psi_{11}A_1\omega - \psi_{12}A_2\omega,$$

$$p_{s1} = \psi_{11}\eta_1 P_{a1} + \psi_{12}\eta_2 P_{a2}, \quad q_{s1} = \psi_{11}\eta_1 q_{a1} + \psi_{12}\eta_2 q_{a2}, \tag{B.15}$$

$$u_{s2} = \psi_{21}\eta_1 U_{a1} + \psi_{22}\eta_2 U_{a2} + \psi_{21}B_1\omega + \psi_{22}B_2\omega,$$

$$v_{s2} = \psi_{21}\eta_1 V_{a1} + \psi_{22}\eta_2 V_{a2} - \psi_{21}A_1\omega - \psi_{22}A_2\omega,$$

$$p_{s2} = \psi_{21}\eta_1 P_{a1} + \psi_{22}\eta_2 P_{a2}, \quad q_{s2} = \psi_{21}\eta_1 q_{a1} + \psi_{22}\eta_2 q_{a2}. \tag{B.16}$$

Appendix C. The entries of the matrix $\mathbf{DP_1}$

$$d_{11} = p_{1a1}a_{1x1} + p_{1a2}a_{2x1} + p_{1b1}b_{1x1} + p_{1b2}b_{2x1} + p_{1t}t_{x1},$$

$$d_{12} = p_{1b1}b_{1xd1} + p_{1b2}b_{2xd1} + p_{1t}t_{xd1},$$

$$d_{13} = p_{1a1}a_{1x2} + p_{1a2}a_{2x2} + p_{1b1}b_{1x2} + p_{1b2}b_{2x2} + p_{1t}t_{x2},$$

$$d_{14} = p_{1b1}b_{1xd2} + p_{1b2}b_{2xd2} + p_{1t}t_{xd2},$$

$$d_{15} = p_{1t}t_{xd3},$$

$$d_{16} = p_{1a1}a_{1\tau} + p_{1a2}a_{2\tau} + p_{1b1}b_{1\tau} + p_{1b2}b_{2\tau} + p_{1t}t_\tau + \sum_{j=1}^{2}\psi_{1j}(A_j\cos(\omega t+\tau) - B_j\sin(\omega t+\tau)), \tag{C.1}$$

$$d_{21} = p_{1a1}a_{1x1} + p_{2a2}a_{2x1} + p_{2b1}b_{1x1} + p_{2b2}b_{2x1} + p_{2t}t_{x1},$$

$$d_{22} = p_{2b1}b_{1xd1} + p_{2b2}b_{2xd1} + p_{2t}t_{xd1},$$

$$d_{23} = p_{2a1}a_{1x2} + p_{2a2}a_{2x2} + p_{2b1}b_{1x2} + p_{2b2}b_{2x2} + p_{2t}t_{x2},$$

$$d_{24} = p_{2b1}b_{1xd2} + p_{2b2}b_{2xd2} + p_{2t}t_{xd2},$$

$$d_{25} = p_{2t}t_{xd3},$$

$$d_{26} = p_{2a1}a_{1\tau} + p_{2a2}a_{2\tau} + p_{2b1}b_{1\tau} + p_{2b2}b_{2\tau} + p_{2t}t_\tau + \sum_{j=1}^{2}\psi_{1j}\omega(-A_j\sin(\omega t+\tau) - B_j\cos(\omega t+\tau)), \tag{C.2}$$

$$d_{31} = p_{3a1}a_{1x1} + p_{3a2}a_{2x1} + p_{3b1}b_{1x1} + p_{3b2}b_{2x1} + p_{3t}t_{x1},$$

$$d_{32} = p_{3b1}b_{1xd1} + p_{3b2}b_{2xd1} + p_{3t}t_{xd1},$$

$$d_{33} = p_{3a1}a_{1x2} + p_{3a2}a_{2x2} + p_{3b1}b_{1x2} + p_{3b2}b_{2x2} + p_{3t}t_{x2},$$

$$d_{34} = p_{3b1}b_{1xd2} + p_{3b2}b_{2xd2} + p_{3t}t_{xd2},$$

$$d_{35} = p_{3t}t_{xd3},$$

$$d_{36} = p_{3a1}a_{1\tau} + p_{3a2}a_{2\tau} + p_{3b1}b_{1\tau} + p_{3b2}b_{2\tau} + p_{3t}t_{\tau} + \sum_{j=1}^{2}\psi_{2j}(A_j\cos(\omega t+\tau) - B_j\sin(\omega t+\tau)), \tag{C.3}$$

$$d_{41} = p_{4a1}a_{1x1} + p_{4a2}a_{2x1} + p_{4b1}b_{1x1} + p_{4b2}b_{2x1} + p_{4t}t_{x1},$$

$$d_{42} = p_{4b1}b_{1xd1} + p_{4b2}b_{2xd1} + p_{4t}t_{xd1},$$

$$d_{43} = p_{4a1}a_{1x2} + p_{4a2}a_{2x2} + p_{4b1}b_{1x2} + p_{4b2}b_{2x2} + p_{4t}t_{x2},$$

$$d_{44} = p_{4b1}b_{1xd2} + p_{4b2}b_{2xd2} + p_{4t}t_{xd2},$$

$$d_{45} = p_{4t}t_{xd3},$$

$$d_{46} = p_{4a1}a_{1\tau} + p_{4a2}a_{2\tau} + p_{4b1}b_{1\tau} + p_{4b2}b_{2\tau} + p_{4t}t_{\tau} + \sum_{j=1}^{2}\psi_{2j}\omega(-A_j\sin(\omega t+\tau) - B_j\cos(\omega t+\tau)), \tag{C.4}$$

$$d_{51} = p_{5a3}a_{3x1} + p_{5b3}b_{3x1} + p_{5t}t_{x1}, \quad d_{52} = p_{5t}t_{xd1}, \quad d_{53} = p_{5a3}a_{3x2} + p_{5b3}b_{3x2} + p_{5t}t_{x2},$$

$$d_{54} = p_{5t}t_{xd2}, \quad d_{55} = p_{5b3}b_{3xd3} + p_{5t}t_{xd3},$$

$$d_{56} = p_{5a3}a_{3\tau} + p_{5b3}b_{3\tau} + p_{5t}t_{\tau} - A_3\omega(\sin(\omega t+\tau) - B_3\omega\cos(\omega t+\tau)), \tag{C.5}$$

$$d_{61} = \omega t_{x1}, \quad d_{62} = \omega t_{xd1}, \quad d_{63} = \omega t_{x2}, \quad d_{64} = \omega t_{xd2}, \quad d_{65} = \omega t_{xd3}, \quad d_{66} = 1 + \omega t_{\tau}, \tag{C.6}$$

where

$$a_{1x1} = P_{a1}, \quad a_{2x1} = P_{a2}, \quad a_{3x1} = P_{a3}, \quad b_{1x1} = P_{b1}, \quad b_{2x1} = P_{b2}, \quad b_{3x1} = P_{b3}$$

$$a_{1x2} = Q_{a1}, \quad a_{2x2} = Q_{a2}, \quad a_{3x2} = Q_{a3}, \quad b_{1x2} = Q_{b1}, \quad b_{2x2} = Q_{b2}, \quad b_{3x2} = Q_{b3},$$

$$b_{1xd1} = M_{b1}, \quad b_{2xd1} = M_{b2}, \quad b_{1xd2} = N_{b1}, \quad b_{2xd2} = N_{b2}, \quad b_{3xd2} = M_{b3}$$

$$a_{1\tau} = U_{a1}\cos\tau - V_{a1}\sin\tau, \quad a_{2\tau} = U_{a2}\cos\tau - V_{a2}\sin\tau, \quad a_{3\tau} = U_{a3}\cos\tau - V_{a3}\sin\tau,$$

$$b_{1\tau} = U_{b1}\cos\tau - V_{b1}\sin\tau, \quad b_{2\tau} = U_{b2}\cos\tau - V_{b2}\sin\tau, \quad b_{3\tau} = U_{b3}\cos\tau - V_{b3}\sin\tau, \tag{C.7}$$

$$p_{1a1} = \psi_{11}e_1\cos(\omega_{d1}t), \quad p_{1a2} = \psi_{12}e_2\cos(\omega_{d2}t),$$

$$p_{1b1} = \psi_{11}e_1\sin(\omega_{d1}t), \quad p_{1b2} = \psi_{12}e_2\sin(\omega_{d2}t), \tag{C.8}$$

$$t_{x1} = -\frac{G_{x1}}{G_t}, \quad t_{xd1} = -\frac{G_{xd1}}{G_t}, \quad t_{x2} = -\frac{G_{x2}}{G_t}, \quad t_{xd2} = -\frac{G_{xd2}}{G_t}, \quad t_{xd3} = -\frac{G_{xd3}}{G_t}, \quad t_{\tau} = -\frac{G_t}{G_{\tau}}, \tag{C.9}$$

$$p_{1t} = \sum_{j=1}^{2}\psi_{1j}(e_j((-\eta_j a_j + b_j\omega_{dj})\cos(\omega_{dj}t) - (\eta_j b_j + a_j\omega_{dj})\sin(\omega_{dj}t)) + A_j\omega\cos(\omega t+\tau) - B_j\omega\sin(\omega t+\tau)), \tag{C.10}$$

$$p_{2t} = \sum_{j=1}^{2} \psi_{1j}(e_j((\eta_j^2 a_j - 2\eta_j\omega_{dj}b_j - \omega_{dj}^2 a_j)\cos(\omega_{dj}t) + (\eta_j^2 b_j + 2\eta_j\omega_{dj}a_j - \omega_{dj}^2 b_j)\sin(\omega_{dj}t)) - A_j\omega^2\ \sin(\omega t + \tau) - B_j\omega^2\ \cos(\omega t + \tau)), \tag{C.11}$$

$$p_{3t} = \sum_{j=1}^{2} \psi_{2j}(e_j((-\eta_j a_j + b_j\omega_{dj})\cos(\omega_{dj}t) - (\eta_j b_j + a_j\omega_{dj})\sin(\omega_{dj}t)) + A_j\omega\ \cos(\omega t + \tau) - B_j\omega\ \sin(\omega t + \tau)), \tag{C.12}$$

$$p_{4t} = \sum_{j=1}^{2} \psi_{2j}(e_j((\eta_j^2 a_j - 2\eta_j\omega_{dj}b_j - \omega_{dj}^2 a_j)\cos(\omega_{dj}t) + (\eta_j^2 b_j + 2\eta_j\omega_{dj}a_j - \omega_{dj}^2 b_j)\sin(\omega_{dj}t)) - A_j\omega^2\ \sin(\omega t + \tau) - B_j\omega^2\ \cos(\omega t + \tau)), \tag{C.13}$$

$$p_{5t} = e_3((\eta_3^2 a_3 - 2\eta_3\omega_{d3}b_3 - \omega_{d3}^2 a_3)\cos(\omega_{d3}t) + (\eta_3^2 b_3 + 2\eta_3\omega_{d3}a_3 - \omega_{d3}^2 b_3)\sin(\omega_{d3}t)) - A_3\omega^2\ \sin(\omega t + \tau) - B_3\omega^2\ \cos(\omega t + \tau)), \tag{C.14}$$

where

$$\begin{gathered} G_{x1} = G_{a1}a_{1x1} + G_{a2}a_{2x1} + G_{a3}a_{3x1} + G_{b1}b_{1x1} + G_{b2}b_{2x1} + G_{b3}b_{3x1}, \\ G_{xd1} = G_{b1}b_{1xd1} + G_{b2}b_{2xd1}, \\ G_{x2} = G_{a1}a_{1x2} + G_{a2}a_{2x2} + G_{a3}a_{3x2} + G_{b1}b_{1x2} + G_{b2}b_{2x2} + G_{b3}b_{3x2}, \\ G_{xd2} = G_{b1}b_{1xd2} + G_{b2}b_{2xd2}, \\ G_{xd3} = G_{b3}b_{3xd3}, \end{gathered} \tag{C.15}$$

$$G_t = \sum_{j=1}^{2} \psi_{2j}(e_j((-\eta_j a_j + b_j\omega_{dj})\cos(\omega_{dj}t) - (\eta_j b_j + a_j\omega_{dj})\sin(\omega_{dj}t)) + A_j\omega\ \cos(\omega t + \tau) - B_j\omega\ \sin(\omega t + \tau)) - (e_3(-\eta_3 a_3 + b_3\omega_{d3})\cos(\omega_{d3}t) - (\eta_3 b_3 + a_3\omega_{d3})\sin(\omega_{d3}t)) + A_3\omega\ \cos(\omega t + \tau) - B_3\omega\ \sin(\omega t + \tau)), \tag{C.16}$$

$$G_\tau = \sum_{j=1}^{2} \psi_{2j}(e_j(a_{j\tau}\ \cos(\omega_{dj}t) + b_{j\tau}\ \sin(\omega_{dj}t)) + A_j\ \cos(\omega t + \tau) - B_j\ \sin(\omega t + \tau)) - (e_3(a_{3\tau}\ \cos(\omega_{d3}t) + b_{3\tau}\ \sin(\omega_{d3}t)) + A_3\ \cos(\omega t + \tau) - B_3\ \sin(\omega t + \tau)), \tag{C.17}$$

where

$$G_{a1} = \psi_{21}e_1\ \cos(\omega_{d1}t), \quad G_{a2} = \psi_{22}e_2\ \cos(\omega_{d2}t), \quad G_{a3} = -e_3\ \cos(\omega_{d3}t), \tag{C.18}$$

$$G_{b1} = \psi_{21}e_1\ \sin(\omega_{d1}t), \quad G_{b2} = \psi_{22}e_2\ \sin(\omega_{d2}t), \quad G_{b3} = -e_3\ \sin(\omega_{d3}t). \tag{C.19}$$

References

[1] P.J. Holmes, The dynamics of repeated impacts with a sinusoidally vibrating table, *Journal of Sound and Vibration* 84 (2) (1982) 173–189.

[2] S.W. Shaw, A periodically forced piecewise linear oscillator, *Journal of Sound and Vibration* 90 (1) (1983) 129–155.

[3] S.W. Shaw, P.J. Holmes, A periodically forced impact oscillator with large dissipation, *Journal of Applied Mechanics* 50 (1983) 849–857.

[4] S.W. Shaw, P.J. Holmes, Periodically forced linear oscillator with impacts: chaos and long-period motions, *Physical Review Letters* 51 (8) (1989) 623–626.

[5] G.S. Whiston, Global dynamics of a vibro-impacting linear oscillator, *Journal of Sound and Vibration* 115 (2) (1987) 303–319.

[6] G.S. Whiston, Singularities in vibro-impact dynamics, *Journal of Sound and Vibration* 152 (3) (1992) 427–460.

[7] R.P.S. Han, A.C.J. Luo, W. Deng, Chaotic motion of a horizontal impact pair, *Journal of Sound and Vibration* 181 (2) (1995) 231–250.

[8] C. Budd, F. Dux, The effect of frequency and clearance vibrations on single-degree-of-freedom impact oscillators, *Journal of Sound and Vibration* 184 (3) (1995) 475–502.

[9] S.W. Shaw, The dynamics of a harmonically excited system having rigid amplitude constraints, Part 1: subharmonic motions and local bifurcations, *Journal of Applied Mechanics* 52 (1985) 453–458.

[10] S.W. Shaw, The dynamics of a harmonically excited system having rigid amplitude constraints, Part 2: chaotic motions and global bifurcations, *Journal of Applied Mechanics* 52 (1985) 459–464.

[11] A.C.J. Luo, Period-doubling induced chaotic motion in the LR model of a horizontal impact oscillator, *Chaos, Solitons and Fractals* 19 (2004) 823–839.

[12] G.W. Luo, Period-doubling bifurcations and routes to chaos of the vibratory systems contacting stops, *Physics Letters A* 323 (2004) 210–217.

[13] G.W. Luo, J.H. Xie, Hopf bifurcation of a two-degree-of-freedom vibro-impact system, *Journal of Sound and Vibration* 213 (3) (1998) 391–408.

[14] G.W. Luo, J.H. Xie, Hopf bifurcations and chaos of a two-degree-of-freedom vibro-impact system in two strong resonance cases, *International Journal of Non-Linear Mechanics* 37 (2002) 19–34.

[15] A. Stefanski, Estimation of the largest Lyapunov exponent in systems with impacts, *Chaos, Solitons and Fractals* 11 (2000) 2443–2451.

[16] S.L.T. de Souza, I.L. Caldas, Calculation of Lyapunov exponents in systems with impacts, *Chaos, Solitons and Fractals* 19 (2004) 569–579.

[17] S.L.T. de Souza, I.L. Caldas, Controlling chaotic orbits in mechanical systems with impacts, *Chaos, Solitons and Fractals* 19 (2004) 171–178.

[18] S.L.T. de Souza, I.L. Caldasa, R.L. Vianab, J.M. Balthazarc, R.M.L.R.F. Brasil, Impact dampers for controlling chaos in systems with limited power supply, *Journal of Sound and Vibration* 279 (2005) 955–967.

[19] D.J. Wagg, Rising phenomena and the multi-sliding bifurcation in a two-degree of freedom impact oscillator, *Chaos, Solitons and Fractals* 22 (2004) 541–548.

[20] W.C. Ding, J.H. Xie, Dynamical analysis of a two-parameter family for a vibro-impact system in resonance cases, *Journal of Sound and Vibration* 287 (2005) 101–115.

[21] A.C.J. Luo, L. Chen, Periodic motions and grazing in a harmonically forced, piecewise, linear oscillator with impacts, *Chaos, Solitons and Fractals* 24 (2005) 567–578.

[22] G.L. Wen, Codimension-2 Hopf bifurcation of a two-degree-of-freedom vibro-impact system, *Journal of Sound and Vibration* 242 (3) (2001) 475–485.

[23] G.W. Luo, J.H. Xie, Codimension two bifurcation of periodic vibro-impact and chaos of a dual component system, *Physics Letters A* 313 (2003) 267–273.

[24] W.C. Ding, J.H. Xie, Dynamical analysis of a two-parameter family for a vibro-impact system in resonance cases, *Journal of Sound and Vibration* 287 (2005) 101–115.

[25] J.H. Xie, W.C. Ding, Hopf–Hopf bifurcation and invariant torus $\mathbf{T}^2$ of a vibro-impact system, *International Journal of Non-Linear Mechanics* 40 (2005) 531–543.

[26] W.C. Ding, J.H. Xie, Torus $\mathbf{T}^2$ and its routes to chaos of a vibro-impact system, *Physics Letters A* 349 (2006) 324–330.

[27] W.C. Ding, J.H. Xie, Q.G. Sun, Interaction of Hopf and period doubling bifurcations of a vibro-impact system, *Journal of Sound and Vibration* 275 (5) (2004) 27–45.

[28] Y. Yue, J.H. Xie, Symmetry and bifurcations of a two-degree-of-freedom vibro-impact system, *Journal of Sound and Vibration* 314 (2008) 228–245.

[29] Y.A. Kuznetsov, *Elements of Applied Bifurcation Theory*, second ed., Springer, New York, 1998.